A weather pattern classification system for regional climate downscaling of daily precipitation

Departamento de Ciencias de la Computación
Facultad de Ciencias Exactas y Naturales

Septiembre de 2008

Tesista

Ariel Eugenio D'onofrio

Directores

Dr. Jean-Philippe Boulanger

Dr. Enrique Carlos Segura

Jurados

Dr. Claudio Menéndez

Dr. Juan Santos

Quiero agradecer a mis padres, hermanos y hermana, directores de tesis,
jurados, amigos, y todas las personas que me ayudaron
a realizar este trabajo,
Ariel D'Onofrio.

Resumen

Se desarrolló y calibró un método de clasificación de patrones atmosféricos aplicados sobre estaciones meteorológicas argentinas con el propósito de predecir eventos de precipitación diaria. La técnica de clasificación utilizada esta basada en el algoritmo de k-medias y es aplicada a un conjunto de 17 variables atmosféricas tomadas del reanálisis ERA-40 en el periodo 1979-1999. El conjunto de variables atmosféricas representa los diferentes componentes de la atmósfera, tanto dinámicos, térmicos, como de humedad. Diferentes tests son aplicados para, (i) optimizar el número de observaciones (patrones atmosféricos) por cluster, (ii) encontrar el tamaño del domino espacial de los patrones atmosféricos aplicados a las estaciones, y (iii) encontrar la cantidad de miembros del conjunto de simulaciones estocásticas. Todos los test de sensibilidad son comparados mediante el índice ROC skill score (RSS). Se encontró que el número de observaciones por cluster es óptimo para cantidades mayores a 39, además, que el tamaño de dominio espacial óptimo encontrado (~4°x4°), es mas cercano a representaciones locales que de escala sinóptica, debido seguramente al rol dominante de las componentes de humedad en la optimización de la función de transferencia. Efectivamente, cuando se reducen el conjunto de variables a un subconjunto de variables sólo con componentes dinámicos, la capacidad predictiva del método se reduce significativamente, y al mismo tiempo el tamaño de dominio debe ser aumentado. Una posible mejora a nuestro método debería considerar entonces la utilización de diferentes tamaños de dominio entre las variables dinámicas y no dinámicas. Se observó que el número de miembros por conjunto de simulaciones debe ser siempre alrededor de dos a tres veces más grande que el número de observaciones promedio por cluster (infiriendo que al menos todos los patrones atmosféricos observados deben ser elegidos por algún miembro del

conjunto). A pesar de que Argentina es un país con una gran variedad de climas (desde tropical en el norte hasta de latitud media y alta en el sur), nuestros parámetros encontrados son validos sobre todo el país. Esto se debe al gran conjunto de variables consideradas para definir los patrones atmosféricos, a medida que el peso de cada una de las variables va variando sobre la función de transferencia de acuerdo al lugar geográfico. Se ha encontrado que la capacidad del método estadístico para predecir eventos de precipitación diaria es bastante homogénea en todo el país para diferentes cantidades de precipitación incluyendo la representación de eventos de precipitación extrema.

Como último, se efectúa una comparación entre el método y diferentes modelos de downscaling climáticos regionales, para tres meses en particular, (Enero 1971, Noviembre 1986 y Julio 1996) caracterizados por condiciones climáticas anómalas en la parte sur de la Cuenca del Plata, mostrando que tanto el conjunto de modelos regionales como el método estadístico logran reproducir la frecuencia diaria de precipitación para los tres periodos, aunque la mayor parte de los modelos tienden a subestimar la frecuencia de días secos y extremos, y a sobreestimar la frecuencia de los días de poca lluvia a moderada.

El método estadístico será próximamente aplicado sobre las estaciones meteorológicas de la Cuenca del Plata, para poder generar escenarios futuros de cambio climático. Dentro de las posibles mejoras al método se puede incluir la división en diferentes dominios de acuerdo al tipo de variable utilizada (dinámica y no dinámica) y una posible evolución temporal del patrón atmosférico (patrón atmosférico correspondiente al día de la predicción, más uno o más patrones atmosféricos correspondientes a los días previos para poder representar la evolución del estado atmosférico).

Abstract

A weather pattern clustering method is applied and calibrated to Argentinean daily weather stations in order to predict daily precipitation data. The clustering technique is based on k-means and is applied to a set of 17 atmospheric variables from the ERA-40 reanalysis covering the period 1979-1999. The set of atmospheric variables represent the different components of the atmosphere (dynamical, thermal and moisture). Different sensitivity tests are applied (i) to optimize the number of observations (weather patterns) per cluster, (ii) the spatial domain size of the weather pattern around the station and (iii) the number of members of the stochastic ensembles. All the sensitivity tests are compared using the ROC skill score (RSS). First, we found the number of observations per cluster to be optimum for values larger than 39. Second, the spatial domain size (~ 4°x4°) was found to be closer to a local scale than to a synoptic scale, certainly due to a dominant role of the moisture components in the optimization of the transfer function. Indeed, when reducing the set of variables to the subset of dynamical variables, the predictive skill of the method is significantly reduced, but at the same time the domain size must be increased. A potential improvement of the method may therefore be to consider different domains for dynamical and non-dynamical variables. Third, the number of members per ensembles of simulations was estimated to be two to three times larger than the number of observations per cluster (meaning that at least all the observed weather patterns are selected by one member). Although Argentina is a country with a variety of climates (from tropical in the north to sub Antarctic in the south), our parameter optimization is found to be valid all over the country. This may be due to the large set of variables considered to define the weather patterns, as the actual weight of the variables in the transfer function certainly varies according to the location. The skill of the statistical method

to predict daily precipitation is found to be relatively homogeneous all over the country for different thresholds of precipitation, including the representation of extreme events. Lastly, a comparison between different regional climate models and the statistical downscaling technique in simulating three months, (January 1971, November 1986 and July 1996) characterized by anomalous climate conditions in the southern La Plata Basin was performed, showing that the models' ensemble and the statistical technique succeed in reproducing the overall observed frequency of daily precipitation for all periods, but most models tend to underestimate the frequency of dry and heavy precipitation days, and also tend to overestimate the frequency of light and middle precipitation events. The statistical method presented in this study will be applied in a near future to the La Plata Basin weather stations in order to provide climate change scenarios. Improvements of the method may include the selection of different domains according to the variables (dynamical and non-dynamical) and a temporal evolution of the weather pattern (day of the prediction and one to more previous days to represent the trajectory of the atmospheric states).

Index

I. Introduction

Throughout the last two decades the field of climate modelling has notably progressed. In particular, the performance of General Circulation Models (GCMs) has been significantly increasing. These models represent the behaviour of the different components of the atmosphere and ocean such as wind, temperature, humidity, from sea level up to 64 km height on discrete grid points covering the totality of the earth. Nowadays the models can simulate fairly well the large-scale features of climate but unfortunately, their coarse spatial resolution (typically in the range from 15,000 to 160,000 km^2) leaves unresolved important sub-grid scale features such as clouds, small-scale thermodynamic interactions and topography, often leading to local and regional discrepancies between models and observations. In particular, it does not allow them to properly represent local daily variability and extreme events, crucial for local impact studies. Downscaling methodologies have been developed with the purpose of filling the resolution gap between GCMs and regional and local scale prediction needed for extreme event studies and impact assessment (see for instance *Menendez et al. 2008*). The aim of atmospheric downscaling is to use GCMs atmospheric variables as a starting point to obtain regional or local scale surface variables such as temperature and precipitation. Basically, downscaling methodologies can be divided into two main threads of investigation, dynamical and statistical. Dynamical downscaling (DDS) uses the information provided by GCMs as a boundary condition to generate a higher resolution regional model (RCMs) over the region of interest. This methodology allows adding important regional information to the model such as topography, soil moisture and, more generally, surface land use and land cover. On the other hand, statistical downscaling (SDS) seeks for a relationship (called transfer function) between observed local climatic variables and large-scale circulation variables of the GCMs. Statistical techniques have proven to be as successful as dynamical techniques, being also far less computationally expensive and simpler to develop (e.g.

Gutierrez et al.,2004; Hewitson, 2006). However, their major drawbacks are their tendency to underestimate extreme precipitation events, and their incapacity in predicting non-stationary behaviours in the transfer function (especially under climate and land-use/land-cover changing conditions). While the stationary issue is a real limitation of SDS application to climate change projections, new methods based on GCM weather pattern analysis can provide insights on its probability of occurrence (*Vrac et al. 2007*). Linear regression and stepwise regression are very popular among the SDS techniques, but they can only be used to predict variables that are not discreet, such as temperature, and are not suitable for daily precipitation since linearity assumption for stochastic variables is way too far from reality. For this reason, other SDS approaches have been developed, such as classification and regression trees (*CART; Hughes et. al., 1993*) and clustering techniques (k-means, *Gutierrez et al., 2004*; neural networks, (*Hewitson, 2006)*; analogues and nearest-neighbours; (*Mehrotra and Sharma, 2005*). Data clustering is a non-linear technique that covers fields of statistical analysis, machine learning, data mining, patter recognition, neural networks, and fuzzy theory. Clustering techniques on SDS generate a partition of the data set into subsets called clusters, each cluster consisting of similar weather patterns linked with its daily rainfall values. The intuitive idea behind clustering is that precipitation occurring during a specific period of time (e.g. one day) with a particular weather pattern (which dimension has to be optimized) tends to be similar as to the precipitation observed another day that has a similar weather pattern. This concept was first explored by *Lorenz (1969)*. It must be noticed that the performance of a classifier for downscaling depends on three factors: the amount of data available for training, the problem difficulty, and the generalization skill for prediction of the classifier.

An advantage of SDS based on classification is that it can handle missing data at weather station very well, making it suitable for Argentina where some stations have gaps of

information. As *Hewitson and Crane (2006)* pointed out, there is empirical evidence that no best statistical technique may exist and that the skill of the different approaches varies with the location and accuracy of the training GCM weather pattern data. This means that a statistical method is locally calibrated and valid. Our objective is to develop and calibrate a statistical downscaling method which will be used in future studies to project climate change scenarios in Argentina and in particular La Plata Basin.

In this study, we analyze the strengths and weaknesses of a statistical method based on clustering techniques, using atmospheric variables from ERA-40 re-analysis and observational data from Argentine stations covering a wide range of climates. While specific variables may have different weights among the large region under study, our objective is to develop a tool, which will then be used for tropical, mid- or high-latitude stations. The study is organized as follows*:* *Section 2* describes the atmospheric- and station data; *Section 3* introduces the general characteristics of the downscaling method; Section 4 discusses the model sensitivity to parameters such as the sensitivity to the clustering technique (we compared neural networks and k-means methods), the weather pattern domain size (optimal synoptic scale), the number of clusters (optimal number of observations per cluster) and the size of the ensemble when predicting daily precipitation (stability of the ensemble prediction); *Section 5* discusses the daily precipitation simulation results at different sites of Argentina and *Section 6* compares the results obtained with several dynamical downscaling regional models; Finally, conclusions are provided in *section 7* together with some perspectives of improvement and application in the framework of the 2008-2012 CLARIS LPB European Project.

II. Data

ECMWF data. The observational data used is the reanalysis ERA-40 dataset provided by the *European Centre for Medium-Range Weather Forecasts* (ECMWF). Reanalysis data is a global dataset describing the state of the atmosphere, which is constructed using a GCM that includes the assimilation of observational data. The reanalysis are the closest gridded representation of recent historical climate available. The regular grid resolution of ERA-40 is of 1.125° latitude x 1.125° longitude and the data consist of four atmospheric variables at different atmospheric levels per day (00:00, 06:00, 12:00, 18:00 h UTC) listed in Tables 1 and 2. For further information about this variables see Appendix A: Atmospheric variables description.

Table 1: *ERA-40 reanalysis list of predictor variables utilized in this study.*

Variable	**Milibar level**
U component wind (U)	200,500,700,850
V component wind (V)	200,500,700,850
Relative humidity (rh)	750,850
Specific humidity (q)	750,850
Vertical velocity (W)	500,700
Geopotential (Z)	500

Table 2: *ERA-40 two dimensional variables.*

Variable	
Total column water	(tcw)
Mean sea level pressure	(msl)

Given that weather station data are only available on a daily time step, only averaged atmospheric field daily values were considered. The ECMWF data used in the following cover the period starting in 1979 (the main reason of this choice is the assimilation of satellite data starting in that year, which provides more reliable data) and finalizing in year 1999,

representing a total of 7670 days. As in *Cavazos (2000) and Cavazos and Hewitson (2005),* the selection of ERA-40 atmospheric predictors for daily precipitation is based on the rationale that they must either be dynamical, or non-dynamical components (thermal or moisture). The dynamical components are captured by the wind fields (U, V at the four levels 200, 500, 700 and 850mb), the geopotential height (Z) at 500mb, the vertical velocity (w) at 500mb (for subsidence and convection) and the mean sea-level pressure (msl). Finally, the moisture component is represented by the relative (rh) and specific (q) humidity at low-levels (850 and 700) and by the total column water (tcw). Although long, the list could also include other variables such the 500-1000hPa thickness or convection indices. However, we found the system to be relatively stable for a large subset of the previous list, demonstrating that the method used in the following allows us to reduce the data space avoiding the redundancy of predictors, and that the list is exhaustive enough.

Argentine weather station data. Daily precipitation time series at 39 Argentine stations covering the period 1959-2001 are used in this study. The Argentine stations analyzed are located all over the country and have been quality-controlled before entering the CLARIS[1] database. Figure 1 shows the stations used and Table 3 gives their name, latitude, longitude and the number of missing daily data over the 1979-1999 period. Stations were subject to statistical tests to check for artificial jumps, outliers and trends in the monthly series *(Buishand, 1982).*

[1] For further information about CLARIS project see: http://www.claris-eu.org/

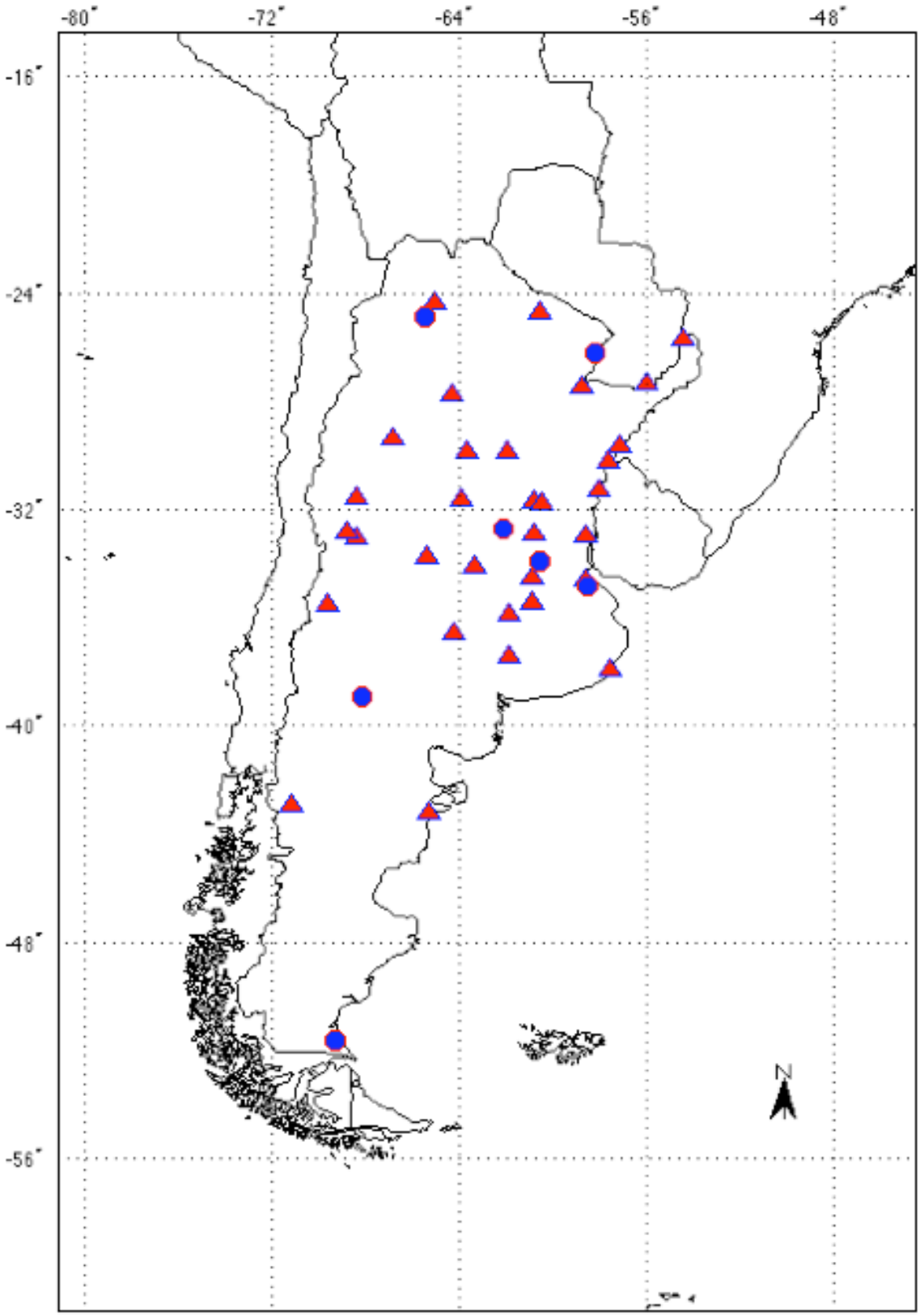

Figure 1: *Map of the 39 Argentinean stations. Blue circles are stations used for model parameter estimations.*

Table 3: List of Argentine stations.

Station Name	**Longitude**	**Latitude**	**Station number**	**Missing days**
'JUJUY AERO'	294.91	-24.38	87046	31
'SALTA AERO'	294.51	-24.85	87047	0
'LAS LOMITAS'	299.41	-24.7	87078	160
'IGUAZU AERO'	305.53	-25.73	87097	28
'SANTIAGO DEL ESTERO AERO'	295.7	-27.76	87129	0
'FORMOSA AERO'	301.76	-26.2	87162	0
'CORRIENTES AERO'	301.23	-27.45	87166	0
'POSADAS AERO'	304.03	-27.36	87178	31
'LA RIOJA AERO'	293.18	-29.38	87217	0
'VILLA MARIA DEL RIO SECO'	296.31	-29.9	87244	103
'CERES AERO'	298.05	-29.88	87257	0
'PASO DE LOS LIBRES AERO'	302.85	-29.68	87289	0
'SAN JUAN AERO II'	291.58	-31.56	87311	0
'SAUCE VIEJO AERO'	299.18	-31.7	87371	31
'PARANA AERO'	299.51	-31.78	87374	2
'MONTE CASEROS AERO'	302.35	-30.26	87393	0
'CONCORDIA AERO'	301.98	-31.3	87395	30
'SAN MARTIN (MZA)'	291.58	-33.08	87416	158
'MENDOZA AERO'	291.21	-32.83	87418	0
'VILLA REYNOLDS AERO'	294.61	-33.73	87448	5
'MARCOS JUAREZ AERO'	297.85	-32.7	87467	0
'ROSARIO AERO'	299.21	-32.91	87480	1
'GUALEGUAYCHU AERO'	301.38	-33	87497	0
'MALARGUE AERO'	290.41	-35.5	87506	31
'LABOULAYE AERO'	296.63	-34.13	87534	0
'PEHUAJO AERO'	298.1	-35.86	87544	182
'JUNIN AERO'	299.08	-34.55	87548	0
'NUEVE DE JULIO'	299.11	-35.45	87550	20
'EL PALOMAR AERO'	301.4	-34.6	87571	263
'EZEIZA AERO'	301.46	-34.81	87576	0
'SANTA ROSA AERO'	295.73	-36.56	87623	1
'CORONEL SUAREZ AERO'	298.11	-37.43	87637	77
'MAR DEL PLATA AERO'	302.41	-37.93	87692	31
'NEUQUEN AERO'	291.86	-38.95	87715	2
'ESQUEL AERO'	288.85	-42.93	87803	41
'TRELEW AERO'	294.73	-43.2	87828	0
'RIO GALLEGOS AERO'	290.71	-51.61	87925	31
'PERGAMINO INTA'	299.45	-33.93	87484	0
'PILAR'	296.11	-31.66	87349	0

III. The statistical downscaling model

For the purpose of this study, a fully operational downscaling toolbox called CHAC was made. It was written in MATLAB language and works on version 7.1 or higher. It has been tested over windows XP, Mac OS and Linux operating systems. CHAC uses free license SOM toolbox (http://www.cis.hut.fi/projects/somtoolbox/) to operate with Self-Organizing Maps. It also uses the Statistical and Mapping toolbox from MATLAB. CHAC can be downloaded from http://sourceforge.neti/projects/chac.

A description of our statistical downscaling methodology main steps is shown on Figure 2. It is based on the previous work made by *Gutierrez et al. (2004)*. This methodology makes use of a clustering technique to connect atmospheric fields with time series of observed daily precipitation or temperature at local stations. The main stages are data pre-processing, followed by data classification, simulation, and finally, validation. In the following sub sections we will describe these stages and also compare two cluster algorithms and find the optimal parameters for the methodology.

Figure 2: CHAC method description.

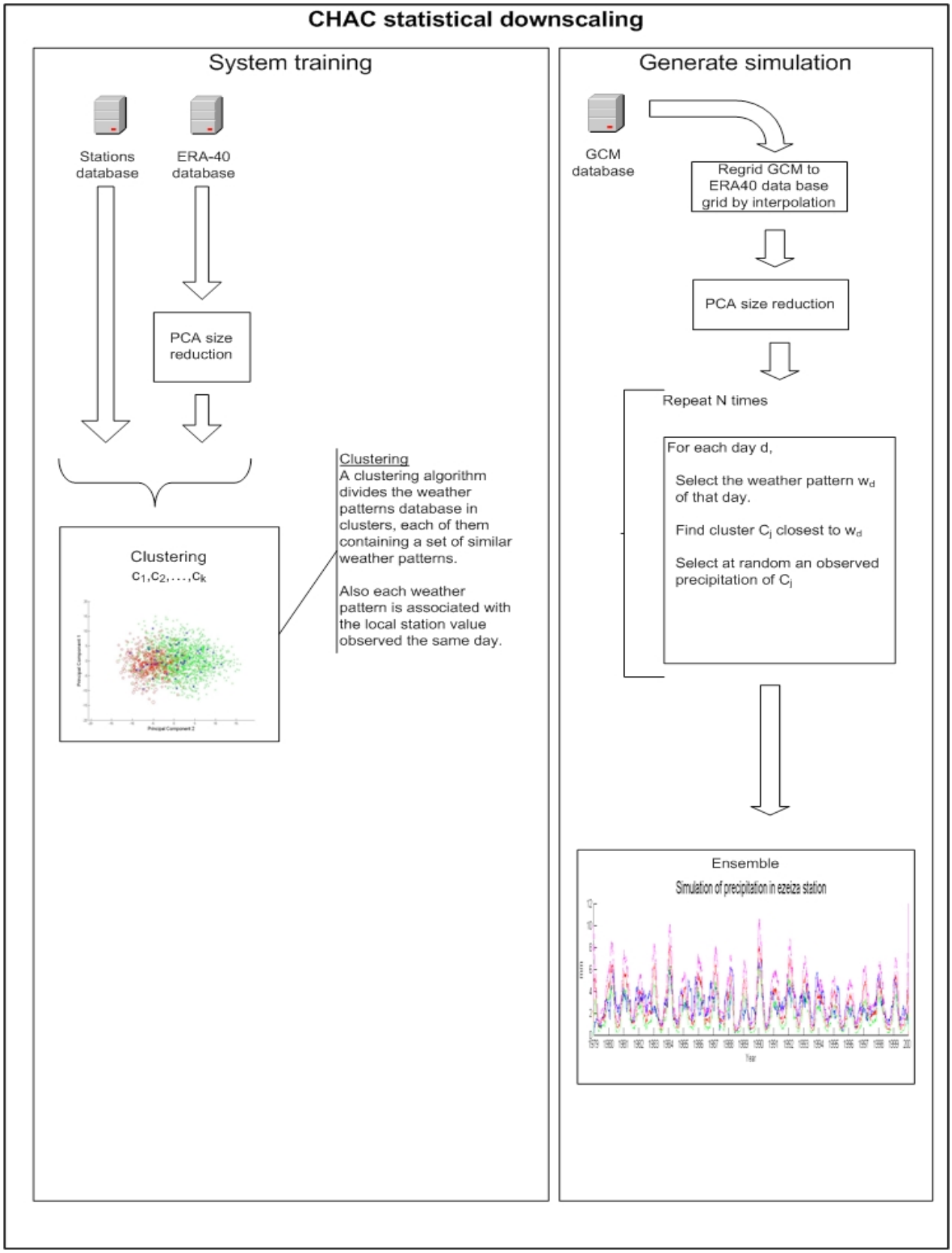

III.a. Data pre-processing

The weather patterns matrix (Wp) is made of 7670 weather pattern vectors, where each vector represents the state of the atmosphere for a given day. This state is specified by the set of 17 ERA-40 variables, listed in tables 1 and 2, in the following way: Every coordinate of each weather pattern vector represents a grid point in the spatial domain of the set of atmospheric variables for a given day. Figure 3 shows an illustration of how the weather pattern matrix is created from spatial domains of 4x4 grid points for temperature at 850mb, relative humidity at 850mb and V wind component at 200mb, for the period 1979-1999.

Figure 3: *7160 weather pattern vectors representing period 1979-1999*

Initial domains: $\forall\, 1 \le k \le 7670$

$$T_k^{850mb} = \begin{pmatrix} t_{11}^k & t_{12}^k \\ t_{21}^k & t_{22}^k \end{pmatrix} ;\ RH_k^{850mb} = \begin{pmatrix} r_{11}^k & r_{12}^k \\ r_{21}^k & r_{22}^k \end{pmatrix} ;\ V_k^{200mb} = \begin{pmatrix} v_{11}^k & v_{12}^k \\ v_{21}^k & v_{22}^k \end{pmatrix}$$

Final weather patterns database:

$$\mathrm{Wp}^{7670,12} = \begin{pmatrix} wp_1 \\ . \\ . \\ . \\ wp_{7670} \end{pmatrix} = \begin{pmatrix} t_{11}^1 & \dots & t_{22}^1 & r_{11}^1 & \dots & r_{22}^1 & v_{11}^1 & \dots & v_{22}^1 \\ . & \dots & . & . & \dots & . & . & \dots & . \\ . & \dots & . & . & \dots & . & . & \dots & . \\ . & \dots & . & .. & \dots & . & . & \dots & . \\ t_{11}^{7670} & \dots & t_{22}^{7670} & r_{11}^{7670} & \dots & r_{22}^{7670} & v_{11}^{7670} & \dots & v_{22}^{7670} \end{pmatrix}$$

In a first step, Wp is normalized (all features have zero mean and unit variance) in order to prevent some atmospheric variables from dominating the following calculations.

In a second step, a Principal Component Analysis (PCA) is performed over Wp. PCA is a well-known statistical linear technique used to compress data by reducing the vector space of the data set in such a way that there is a minimal loss of variance. The motivation for using this technique is the assumption that Wp contains redundant predictors that will not contribute significantly to the quality of the downscaling. PCA first calculates the correlation matrix C^{nxn}

of Wp^{mxn}, with C being symmetric and having $e_1,\ldots,e_n$ eigenvectors, and $\lambda_1,\ldots,\lambda_n$ real eigenvalues. The elements C_{it} represent the covariance between the variables i and t of the original space:

$$c_{it} = \left\langle \left(x_{ki} - u_i\right)\left(x_{kt} - u_t\right) \right\rangle_k \;;$$

$$u_i = \left\langle x_{ki} \right\rangle_k \quad , \quad u_t = \left\langle x_{kt} \right\rangle_k$$

A transformation matrix M^{nxn} is then constructed as follows, each row of M is an eigenvector of C, and they are ordered in decreasing order according to the magnitude of their corresponding eigenvalue. The eigenvalue corresponds to the variance of Wp projected on the eigenvector associated. The coefficients of the elements of Wp projected on the new base are called principal components (PCs^{mxn}).

The matrix calculation to generate the PCs is,

$$PCs = Wp.M^T = \begin{pmatrix} wp_{11} & \ldots & wp_{1n} \\ . & \ldots & . \\ . & \ldots & . \\ wp_{n1} & \ldots & wp_{mn} \end{pmatrix} \begin{pmatrix} e_{11} & \ldots & e_{1n} \\ . & \ldots & . \\ . & \ldots & . \\ e_{n1} & . & e_{nn} \end{pmatrix}$$

This new coordinate representation of the data allows us to select the number of PCs that retain most of the variance, generally reducing the size of Wp matrix up to 90%. This reduction has numerous advantages. Representing the information in a compressed way with a minimal loss of information is important for a classifier task due to the curse of dimensionality: as dimensionality increases the data sample needed to fill the input space grows exponentially, making harder for a classifier to reach a good generalization performance if the same amount of data is available for classification. Also, an immediate reward in the reduction of the data space dimensions is the lower need in computer resources and a faster simulation speed.

III. b. Classification procedure

In a third step, the remaining PCs of the weather patterns are classified. In the following, we will compare the performance of two often-used techniques: k-means (*Gutierrez et al., 2004*) and the SOM (*Self-Organizing Maps; Hewitson and Crane, 2006*). While other methods (analogue and k-nearest neighbors) have also been implemented, we only discuss these two clustering methods, which gave the best results.

III.b.1. K-means classification algorithm

K-means is one of the clustering techniques most widely used. Its success is based on its simplicity and fast convergence speed, making it very appropriate for computer implementation. Lets assume we have a set of patterns, in particular it can be a weather patterns set $X = \{x_1, x_2,\ldots,x_m \mid x_i \in R^n\}$, and a set of centroids $C = \{c_1,c_2,..,c_k \mid c_i \in R^n\}$, then each cluster is defined as all $x_i \in C_k$ such as C_k is the closest centroid to x_i. The k-means technique assumes that the minimum sum of the intra-cluster variance is the best representation of the data and so attempts to minimize the squared error function F_e;

$$F_e = \sum_{i=1}^{k} \sum_{x_j \in C_i} \left\| x_j - C_i \right\|^2$$

A pseudocode of k-means algorithm is shown in Algorithm 1. The k-means algorithm starts by generating the positions of the initial centroids. The simplest method is to make a random selection over the set of input patterns. Then, an iterative adjustment of the centroids positions and reassignment of the patterns x belonging to them is made, until a performance criterion is achieved or a maximum number of iterations is reached.

K-means can be sensitive to the initial random solution, and the search for the minimum intra cluster variance can be easily stuck in local minima, for that reason it is recommended to

repeat the algorithm several times using different initial random centroids, and to chose the solution with the minimum intra cluster variance.

Algorithm 1. *k-means algorithm*

Inputs
    $X = \{x_1,\ldots,x_m\}$
    k : Number of clusters

Outputs
    $C = \{c_1,\ldots,c_k\}$ (cluster centroids)
    $m: I \rightarrow C$ (cluster membership function)

Procedure k-means

    Set C to initial value (e. g. random selection of I)
    For each $x_j \in X$
        $m(x_j) = \underset{q \in \{1,.k\}}{\text{argmin}} \; (\text{distance}(i_j,c_q))$
    end
    While m has changed
        For each $j \in \{1, k\}$
            Recompute C_j as the centroid of $\{x_i \mid m(x_i) = j\}$
        End
        For each $x_j \in X$
            $m(x_j) = \underset{q \in \{1,k\}}{\text{argmin}} \; (\text{distance}(x_j, c_q))$
        End
    End
Return C , m
End

There exists a wide range of distance measures to use in k-means squared error function F_e, we use the squared Euclidean distance, in which each centroid is the mean of the points inside its cluster.

III.b.2. SOM classification algorithm

The other technique used in this study is Kohonen self-organizing feature map (SOM), sometimes also called topology-preserving map. It was created by Teuvo Kohonen in 1982, and is a clustering technique combined with topological preserving and data reduction ordered map properties. It forms part of the non-supervised learning neural network field, which is inspired by the human nervous system. The structure of a SOM consists of two layers (see Figure 4), which are called the input layer and the output (or representation) layer, with feed-forward connections from input to output and lateral connections between neurons in the output layer. The output layer has the shape of a two-dimensional lattice of neurons, but also one or higher dimensional layers can be used, though less common. Each neuron on the output layer has an associated weight vector in the output space. The goal of a SOM is to represent all points in the input space by points in the output space, preserving distance and proximity relationships as much as possible.

Figure 4: *Structure of a SOM*

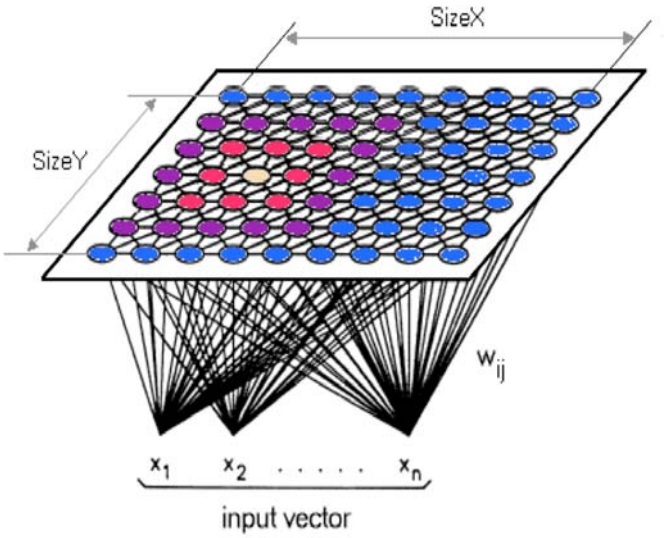

SOM training is more complex than k-means, the learning process consists in the systematic modification of the weight vectors of each neuron in response to input patterns until a stable configuration arises. Unlike other learning technique in neural networks, training a SOM requires no target vector, therefore it learns to classify, reduce dimension, and display similarities among the training data without any external supervision. In order to do this the training data for the SOM algorithm is presented in epochs, being each epoch a complete instance of the input database sorted randomly.

The training algorithm of a SOM can be divided four important stages.

1. Initialization

The weight vectors of each neuron of the SOM are selected at random from the input database.

2. Competition

For each sample vector selected, all neurons in the SOM compute their respective values of discriminant functions. The neuron with the highest value is called de Best Matching Unit (BMU), and is declared the winner of the competition. There are numerous ways to determine the discriminant function, the most commonly used method being the *Euclidean Distance* and/or *Cosine Distance*

3. Cooperation

Once the winning neuron has been selected, a spatial location of neighborhood neurons will be exited to form part of the algorithm. This part of SOM training is neurobiologically inspired. The topological neighborhood is defined by a function $h_{j,i}$ which has to satisfy two specific requirements.

- The topological neighborhood has to be symmetric around the winning neuron.

- The amplitude of the topological neighborhood $h_{j,i}$ decreases monotonically as the lateral distance $d_{j,i}$ increase, decaying to zero for $d_{j,i} \rightarrow \infty$; this is a necessary condition for convergence. The lateral distance is defined in the output space of the SOM and in the case of a two-dimensional lattice it is defined as, $d_{j,i} = \| r_j - r_i \|^2$, where the discrete vector r_j defines the position of exited neuron j and r_i defines the discrete position of winning neuron i. Also The size of the topological neighborhood shrinks with time, a common choice for $h_{j,i}(x)$ is $h_{j,i} = \exp\left(-\frac{d_{j,i}^2}{2\sigma^2}\right)$, being σ the parameter of the function that selects in which intensity the neighborhood function gets involved in the learning process.

4. Synaptic adaptation

The synaptic adaptation mechanism is performed only on the exited neurons selected in the cooperative step. The synaptic adaptation modifies the weights of the selected neurons in such a way that the response of the winning neuron to the subsequent application of a similar input pattern is enhanced.

The updated weight vector $w_j(n+1)$ at step n+1 is defined by,

$$w_j(n+1) = w_j(n) + \eta(n)h_{j,i(x)}(n)(x-w_j(n))$$

Where η is the learning rate parameter ($0 < \eta < 1$), that defines how fast does the updated weight vector gets closer to its sample vector. If η is too high the learning process might not converge, whereas if it is too low it might get trapped in a metastable state: A configuration of the SOM in which it can not learn the statistical distribution of the input data. As a general rule η is monotonically decreasing in time, in this study η

change rule is $\eta(t)= \eta_0/(1+100t/T)$, where η_0 is learning rate initial value, T is the training length in epochs and t is the time step.

The SOM training has two well-defined phases, which are defined by the values of its training parameters, learning rate (η) and neighborhood function (h).

- Ordering phase: In this phase the SOM reproduce the statistical distribution of the learned distribution in a quick way. The learning-rate parameter should begin in a high value, often 0.1 and decrease monotonically but remain above 0.01. The neighborhood function $h_{j,i}(n)$ should include all neurons in the network centered on the winning neuron i and then shrink with time.

- Convergence phase: In this phase the SOM learns the local distributions. The number of iterations should be greater than in the ordering phase, al least 500 times the number of neurons in the network. The learning parameter should be small, in the order of 0.01, but never reach 0, and the neighborhood function $h_{j,i}(x)$ should contain only the closest neurons of a winning neuron, reducing eventually to one o even zero neighboring neurons.

III.c. The simulation procedure

At this stage, the classifier algorithm divides the database of weather patterns into clusters, with the restriction that every weather pattern belongs only to one specific cluster. Given that each daily weather pattern is associated to the precipitation value observed on that day, we can relate a precipitation distribution to each cluster.

When making a simulation with new atmospheric weather patterns as an input, each weather pattern is projected onto the clusters by computing its distance to each of them. Only one cluster is selected (the one to which the distance is smallest). The simulated precipitation

value is selected randomly from the daily precipitation distribution of the selected cluster. If the weather pattern projected also belongs to the cluster, then the precipitation value associated to it is not chosen for simulating that day, in order to avoid over fitting. Considering the stochastic nature of the system, an ensemble of N simulations (a discussion on N is provided hereafter) is generated.

III.d. The validation procedure

A set of standard indices is used to validate the skill of our statistical model, one of which is the ROC curve (Relative Operating Characteristic). A ROC curve is obtained as follows. Let's assume we have a stochastic prediction of size N produced over a specific period. Then N can be divided into two subsets, those when an event occurred and those when it does not, i.e. N=O + O´, see Table 4.

Table 4: *Definition of events such as used when computing the ROC index.*

Observations	**Warning**	**No warning**	**Total**
Event	H	M	O
Non Event	FA	CR	O´
Total	W	W´	N

Let H be the number of hits whenever an event occurred and a warning was issued, let FA be the False Alarm whenever a warning was issued, but no event occurred, let M be the number of missed events, which is the number of times that an event occurred but no warning was issued, and let CR be the number of correct rejections, which is the number of times that an event did not take place and no warning was made. Bearing this in mind, we can calculate the hit rate (number of occurred events well predicted) and false alarm rate (number of events predicted, which actually did not occur) as follows: $HR = \frac{H}{O}$ and $FAR = \frac{FA}{O'}$.

Considering that the simulation is actually an ensemble of N simulations, a critical threshold P_{cr} (e.g. percentage of simulations presenting an event) is introduced and a warning is fired every time the number of simulations presenting an event exceeds this threshold. In this case, the hit and false alarm rates can be expressed as a function of P_{cr} in the following way,

$$HR(P_{cr}) = \Pr\{\Omega_P / E = 1\} = \int_{\Omega_P} f(P/E=1)dP$$

$$FAR(P_{cr}) = \Pr\{\Omega_P / E = 0\} = \int_{\Omega_P} f(P/E=0)dP$$

where Ω_p denotes forecast probabilities P>P_{cr} and $f(P/E)$ is the conditional probability density function of probability forecasts (*Kharin and Zwiers, 2003*)

Finally, the ROC curve is made by plotting the resulting hit rates versus false alarm rates as P_{cr} varies from 0 to 1. In every ROC curve, a forecast with no skill corresponds to the diagonal connecting the points (0,0) and (1,1), and a perfect forecast generates a ROC curve going through the points (0,0), (1,0) and (1,1). Furthermore, in a forecasting system with no skill, the hit-rate and false-alarm rate are equal, and in the case of perfect forecast, hit rate is equal to 1 and false alarm rate equals to 0.

The index mostly used in the present study is the ROC skill score (RSS), which is based on the area under the ROC curve as follows: $RSS = 2*(area - 0.5)$. Then, a no-skill forecast has a ROC area of 0.5 and a RSS equal to 0, and a perfect forecast has a ROC area of 1, and a RSS of 1. Moreover a forecast A is better than a forecast B, if the area under the ROC curve of A is greater than B i.e. if the RSS of A is larger than the one of B. As a final comment, to compare the skill of simulated distributions related to precipitation data, we will display PP-plot and QQ-plots.

PP-plot is built as follows. To each probability of the observed CDF, a certain wet or dry sequence length is associated. For such wet or dry sequence length, we can associate a

probability of the observed CDFs. Such probabilities are then plotted as a scatter plot. Cumulative probabilities are in the range 0-1. The straight line crossing both axes at zero represent a perfect fit. For each plot, we computed a mean algebraic error and the root-mean square of the model-data error misfit.

QQ-plot is built as follows. To each probability of the CDF (both observations and simulations have the same number of points, and thus the same bins of the CDF), we can associate a rainfall amount for observed or simulated series. The two series are then plotted as a scatter plot. Daily rainfall amounts are in the range 0.1-350mm. The straight line crossing both axes at zero represent a perfect fit. For each plot, we computed a mean algebraic error and the root-mean square of the model-data error misfit.

IV. Model parameter choice

In order to test the statistical model parameter choices (clustering technique, number of clusters, domain size, ensemble size), we evaluate the model skill in a subset of seven weather stations representative of very different climate conditions over Argentina (see blue circles in Figure 1). Formosa (Formosa Province) is located at the frontier between Argentina and Paraguay and present a near-tropical climate with very strong convection systems and a well-marked rainy season during the South American Monsoon (austral summer). Salta (Salta Province) is located in the northwest region of Argentina and is characterized by a dry climate. Pergamino (Buenos Aires Province) is in the core region of agriculture production in Argentina. Its annual mean precipitation exceeds 1000mm. Marcos Juarez (Cordoba Province) is a semi-arid region and an agricultural marginal region. However, the increase of precipitation during the last 30 years considerably favoured the growth of cereal crops in the area. Ezeiza (Buenos Aires Province) is an airport station very close to the Capital of

Argentina (Buenos Aires). The climate is influenced by convection during summer and by frontal activities. Monthly precipitation amounts are quite equally distributed during the year (*Boulanger et al., 2005*). Neuquén (Neuquén province) is very close to the Andes and located in a mid-latitude region strongly influenced by frontal activities. Rio Gallegos (Santa Cruz Province) is one of the stations located in the south of Argentina (near 50°S) and is representative of a mid-latitude climate.

This subset of stations is analyzed in details to evaluate the sensitivity of the method to the location of the station and thus develop a method relatively skilful all over the country. For the sake of clarity (and number of figures), in the result section we mostly present averaged ROC scores among the 7 stations.

Clustering technique and number of clusters. Figure 5 displays the ROC score averaged between the 7 selected stations as a function of the number of clusters (actually expressed as the mean number of observations per cluster i.e. number of daily observations divided by the number of clusters) using two different clustering techniques (k-means in red and SOM in blue). Following *Hewitson and Crane (2006),* we selected a domain size on the order of 1000km x 1000 km around each station to extract the atmospheric variables. Ensembles of 100 simulations are performed to compute the RSS. It appears that the k-means mean curve is always higher than the SOM curve suggesting the k-means clustering technique is more effective in covering the data space than SOM. Indeed, the topological order imposed by the SOM method strongly limits the SOM clusters to explore low density regions of the data space (Fig. 6). This property can be also viewed on Fig. 7, in which a SOM lattice of 25x25 was trained for Marcos Juarez in the period 1979-99 and shown in the 3 dimensional input space spanned by the first 3 PCs. Informally speaking, due to its topological order property the SOM tries to fill the statistical distribution of the weather patterns with the constraint of

being a two-dimensional sheet in a n-dimensional space. This behaviour affects the capacity of the SOM to explore the variance of the input data and therefore affects it generalization skill. Although a thorough work on the SOM parameters (not shown on this study) gets similar RSS than k-means, it affected significantly the topological order of the SOM. This reason, and moreover for the good results of the k -means technique, which is fast and easy to implement, lead us to select this method as the clustering method for downscaling..

The training parameters for both SOM and k-means were as follows:

SOM: Neuron initialization at random

Parameters	**Ordering Phase Values**	**Convergence Phase Values**
Initial Radius (σ_i)	max(mapsize)/4	max(*Final Radius*,1)
Final Radius (σ_f)	*Initial Radius*/4	1
Initial Learning Rate(η)	0.5	0.05
Number of Epochs	100	1000
Neighbourhood function	Gaussian	Gaussian

K-means: Cluster initialization at random.

Parameters	**Values**
Maximum number of iterations	100
Number of repetitions of the algorithm	1

In addition, regardless of the clustering technique, it is found that the ROC curve for precipitation occurrence or for different thresholds of precipitation (25%, 50% or 75% of the precipitation CDF) displays a similar shape mostly independent of the station under study. The optimal number of observations per cluster can be estimated to be between 20 and 50 observations, although the decrease in the RSS value is very slow as the number of observations increases, and the differences are not highly significant in terms of daily precipitation simulations. The selected number of observations per cluster is 39 (equivalent to 196 clusters for our dataset). This value is much smaller than the one (90) selected by *Hewitson and Crane (2006)*, but as said above the RSS is not very different for 39 or 90 observations per cluster. A final comparison over this two techniques is made on their speed,

Figure 8, shows the elapsed time of each technique over a set of different number mean observations per cluster. It shows that k-means is faster than SOM for mean observations per cluster lower than 45 and that it is slower for greater values than 45. It must be point out though that time cost may greatly depend on how the algorithms are implemented by each toolbox.

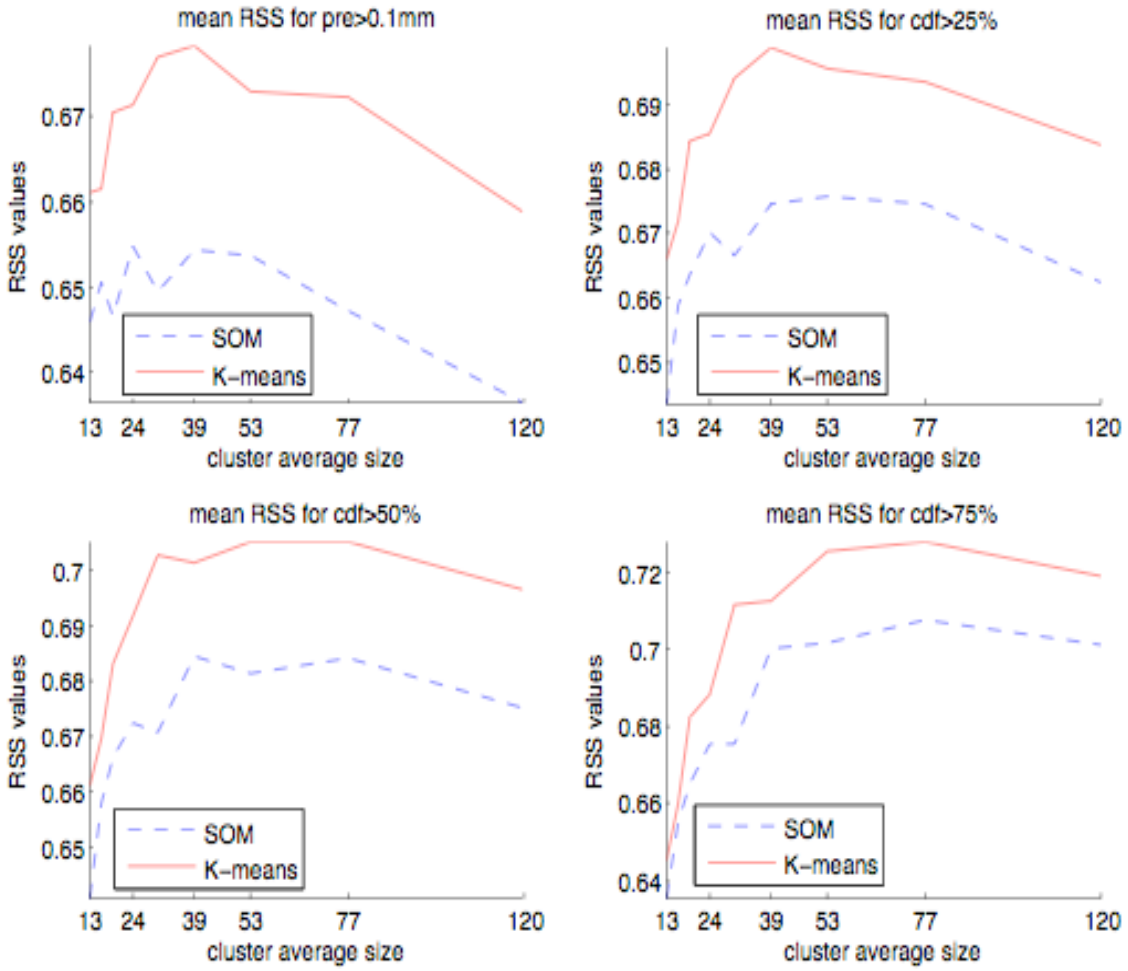

Figure 5: *RSS values averaged over the seven selected stations as a function of the mean number of observations per cluster. The blue curve represents results from the SOM classification, while the red curve represents results from the K-means classification. The RSS score is computed for four different criteria: (upper-left) wet/dry day; (upper-right) daily amount larger than the 25th percentile of the rainfall amount cumulative distribution function (CDF); (lower-left) daily amount larger than the 50th percentile; (lower-right) daily amount larger than the 75th percentile.*

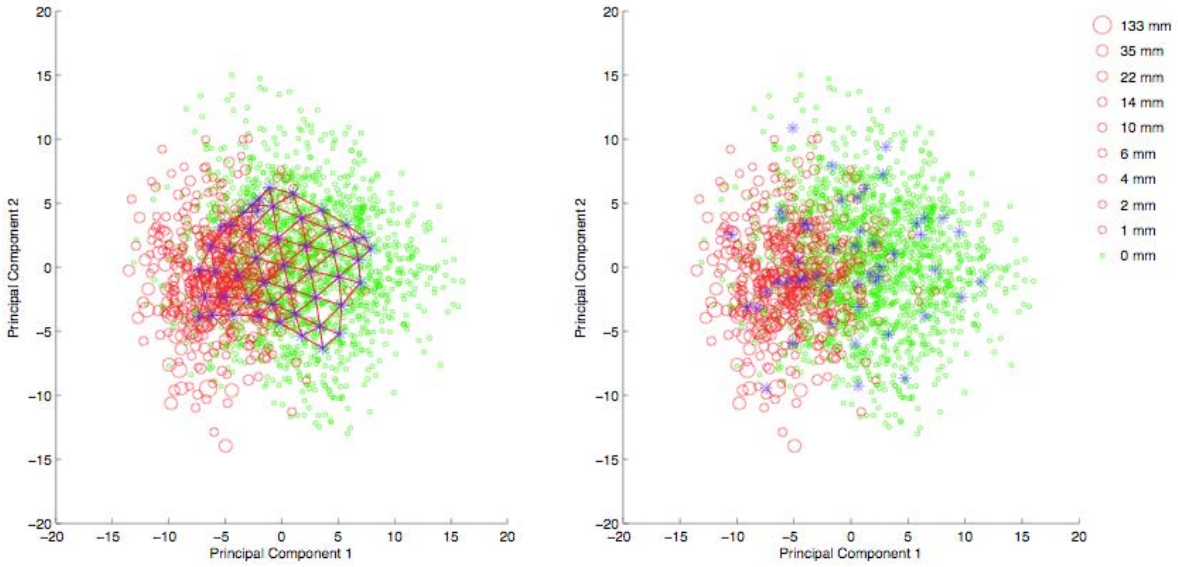

Figure 6: *Representation of the cluster nodes (blue stars) computed by the SOM (left) or K-means (right) technique) in the two-dimensional space of the first two principal components of the data space for the station Marcos Juarez in period 1990-1996. The green dots represent dry days, red circles represent wet days, and the size of the red circles is a function of the intensity of the daily rainfall.*

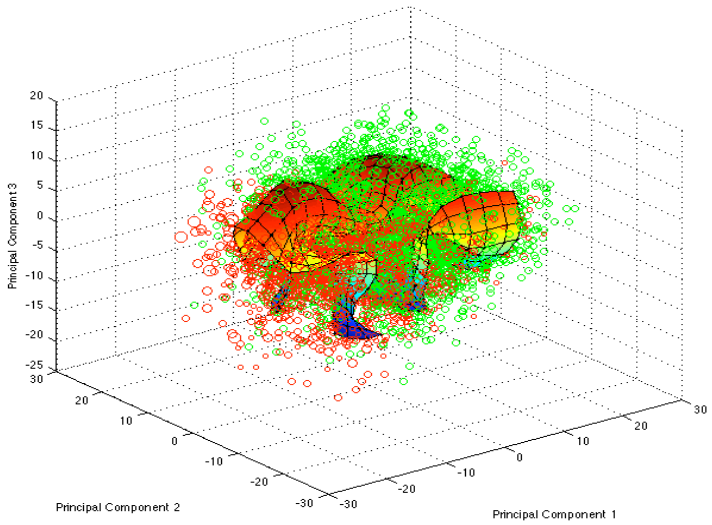

Figure 7: *Representation of the SOM over the 3 dimensional space of the first three principal components of the weather patterns space for the station Marcos Juarez. In here, it can be noticed that SOM behaves like a 2 dimensional lattice trying to represent the 3 dimensional statistic distribution of the data space.*

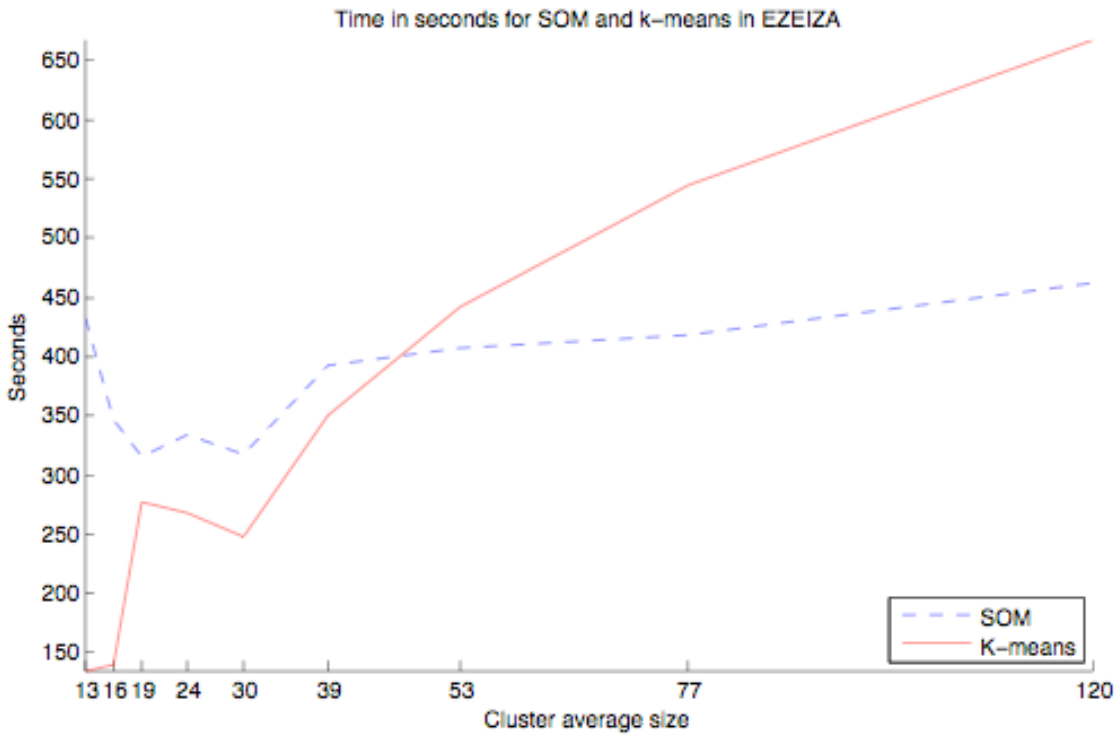

Figure 8: *Plot of the clustering time in seconds for SOM and k-means for different number of initial clusters. The algorithms where performed over Ezeiza PCs database weather patterns matrix of size 7670x43, representing period 1979-1999.*

Domain size. Given the previous result, at each of the seven stations, daily weather patterns are defined for different spatial domain sizes and then clustered. Ensembles of 200 simulations are performed to compute the RSS scores. In the following, we will define 1x1 as the vertical at the grid point the closest to the weather station, 2x2 as the four nearest grid points to the station, 4x4 as the 16-grid point square including the 2x2 square, 6x6 as the 36-grid point square including the 4x4 area, etc. In terms of spatial resolution, 1x1 is a profile, 2x2 is a 1.125° size square, 4x4 is a 3.375° size square, 6x6 is a 5.625° size square etc. Thus, we computed the RSS-averaged score from the RSS scores at all seven stations for four different RSS criteria (0.1mm/day, 25%, 50%, and 75% of the station CDF distribution). The results are displayed in Figure 9. While the RSS value is of similar amplitude for domains smaller than 6x6, the large domains (8x8 and larger) present decreasing RSS values. The RSS value of the vertical profile (1x1) is always found to be smaller than the 2x2, 4x4 or 6x6

domain sizes, meaning that local- to synoptic-scale information improves the relationship between atmospheric conditions and precipitation simulation at the weather station.

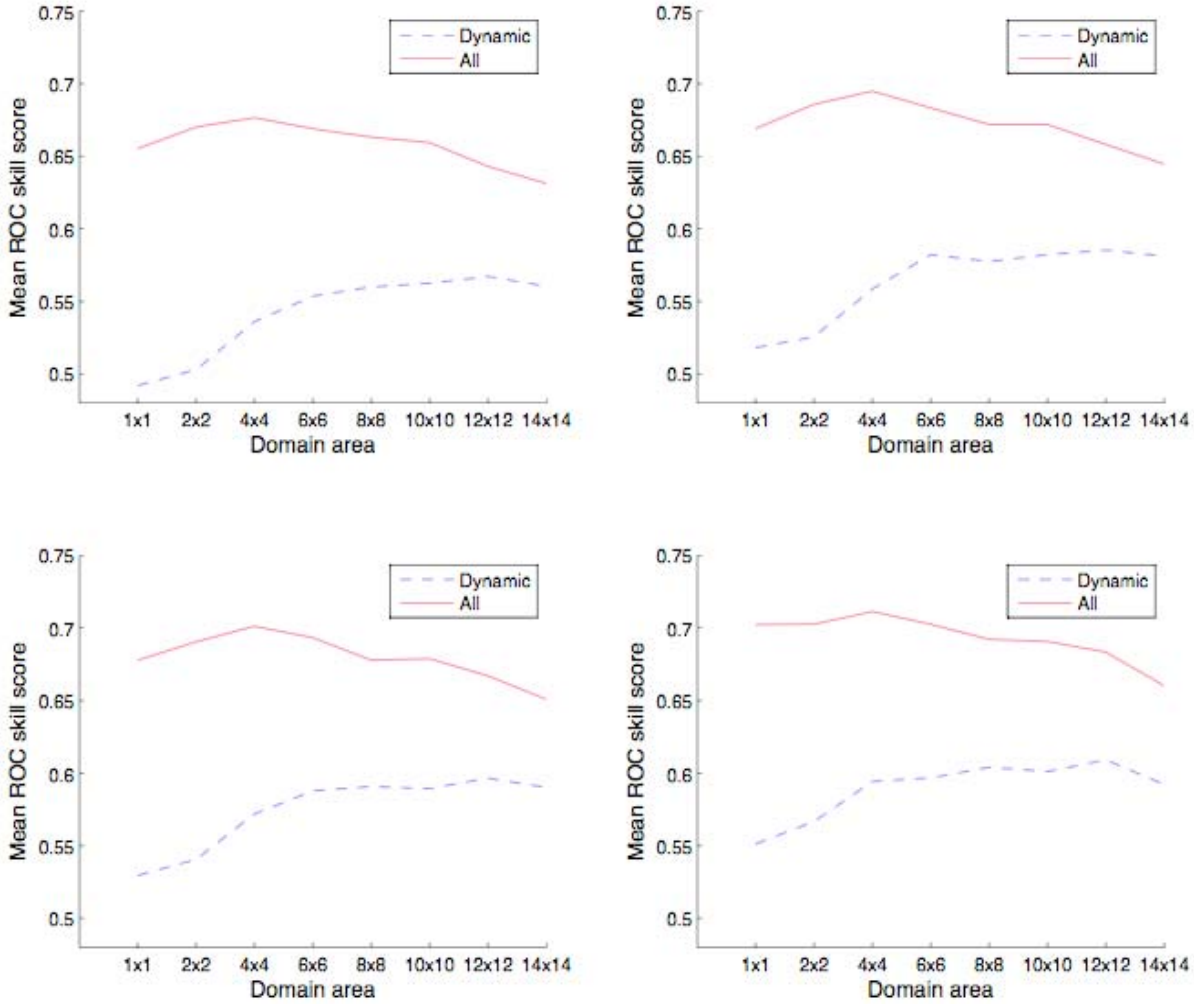

Figure 9*: ROC skill score (RSS) averaged over the seven selected stations as a function of the domain area around the station. The red curve represents results when using all the dynamical and non-dynamical variables. The blue curve represents results when using only dynamical variables. RSS is computed for four different criteria: (upper-left) wet/dry day; (upper-right) daily amount larger than the 25th percentile of the rainfall amount cumulative distribution function (CDF); (lower-left) daily amount larger than the 50th percentile; (lower-right) daily amount larger than the 75th percentile.*

We finally decided to select a 4x4 domain size (3.375° x 3.375°). Therefore, our result highlights a very small-radius of atmospheric variability around the station suggesting a

strong role of moisture components in the weather pattern clustering. Indeed, if the atmospheric variables are only dynamical variables (blue curve in Figure 9), the optimum domain size is larger and extends up to 10x10 or 12x12 domain sizes highlighting the importance of larger scale patterns to define dynamical weather patterns. However, it is worth pointing out that the RSS values of the method, when based only on dynamical variables, are significantly smaller than the RSS values of the method when based on the dynamical and non-dynamical atmospheric variables. This suggests that even if the large-scale circulation is clearly a strong constraint on local precipitation, what defines ultimately the occurrence and amplitude is strongly related to non-dynamical local- and synoptic-scale processes.

Ensemble size. Here we are interested in analyzing the sensitivity of the RSS calculation to the number of simulations of the ensemble, in order to reduce the computational time without losing predictive skill. In Figure 10, the RSS averaged between the 39 stations is displayed for different types of events (P>0.1mm/day, > 25%, 50% or 75% of the wet days distribution), for an ensemble size of 200 members. Briefly, it appears that the computation of the RSS converges for 100 simulations or more per ensemble. In fact, we found (for different experiments not shown here) that the convergence happens for a number of simulations 2 to 3 times the average number of observations per cluster. This can easily be explained by the fact that the weather patterns have been selected at least twice in the ensemble. Therefore, we choose to do the simulations with all ensembles having 100 members, even if very small improvements (~0.01) in the RSS could be reached when doubling the number of simulations.

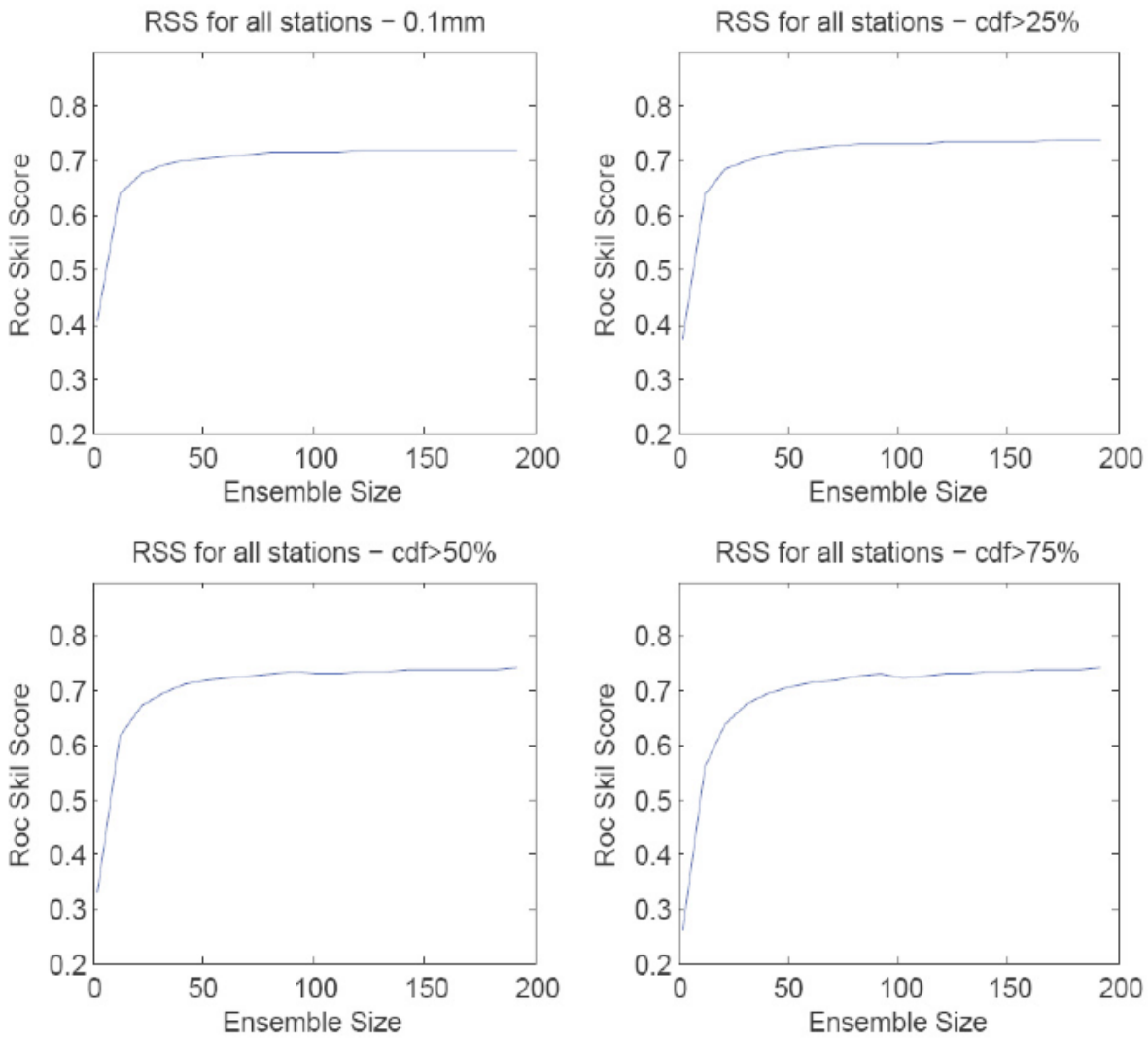

Figure 10: *ROC skill score (RSS) averaged over the 39 stations as a function of the ensemble size, from 2 to 200 simulations. RSS is computed for four different criteria: (upper-left) wet/dry day; (upper-right) daily amount larger than the 25th percentile of the rainfall amount cumulative distribution function (CDF); (lower-left) daily amount larger than the 50th percentile; (lower-right) daily amount larger than the 75th percentile.*

V. Model skill in Argentina

In order to evaluate the general skills of the method over the entire database, we defined four types of daily events at each station instead of defining precipitation events in terms of a threshold in mm/day identical for all stations. These events are wet days (amount larger than 0.1mm/day) and precipitation amounts larger than 25%, 50% or 75% of the amount

distribution. These thresholds are proper to each station in order to compute the number of events predicted. Then the hit rates and false alarm rates are computed over all the stations in order to derive the ROC curve and the RSS. As displayed in Figure 11, whatever the threshold considered, the RSS is around 0.72 highlighting the good results of the statistical method for both low and large rainfall amounts.

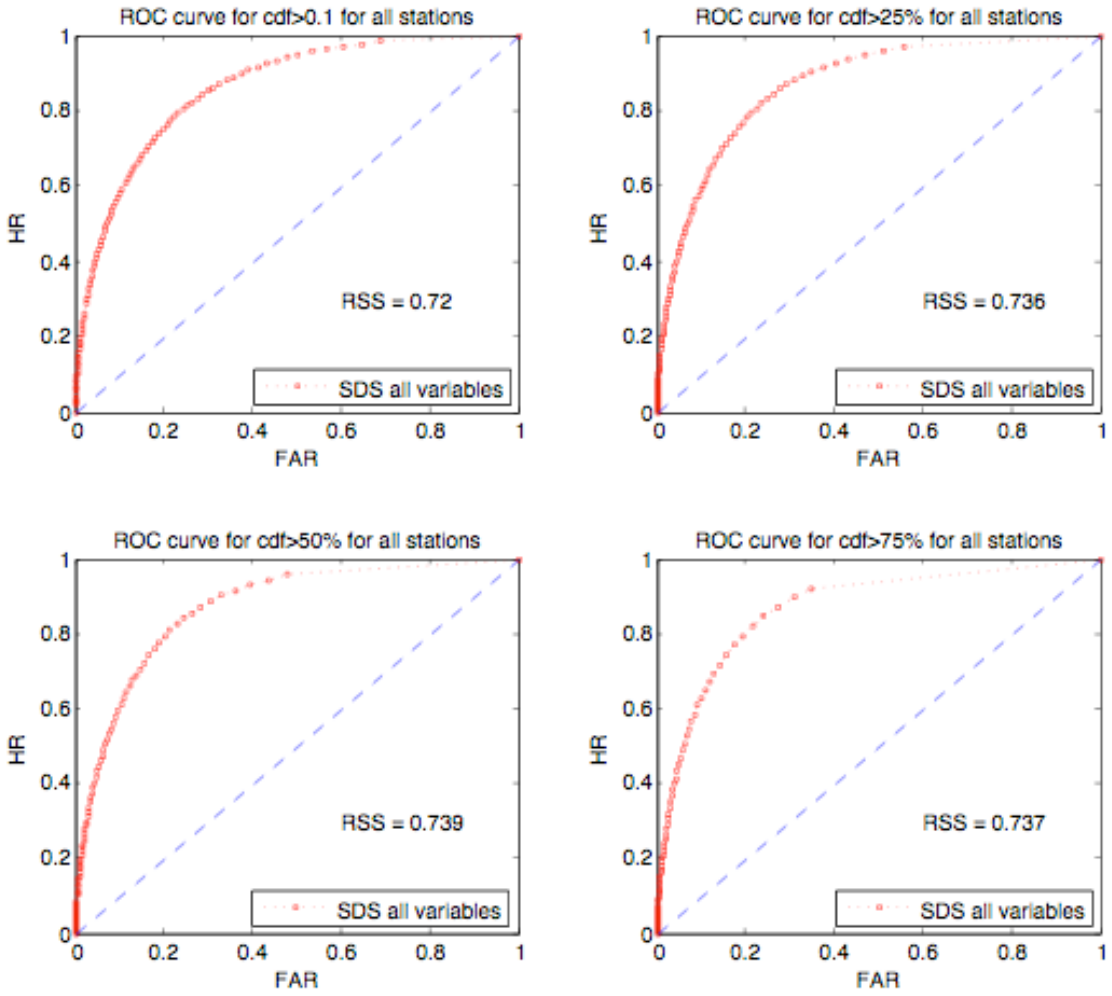

Figure 11: ROC curve computed from all the stations in the database. The ROC curve is computed for four different criteria: (upper-left) wet/dry day; (upper-right) daily amount larger than the 25th percentile of the rainfall amount cumulative distribution function (CDF); (lower-left) daily amount larger than the 50th percentile; (lower-right) daily amount larger than the 75th percentile.

Moreover, our method of computing events relative to a percentile of the rainfall amount distribution ensures that the RSS is indeed representing the skill of the method over all stations to simulate local rainfall amounts. Computing the RSS for events larger than for

example 10mm/day would, for a country like Argentina, reduce the evaluation of the model skills to wet regions. In order to study climate impacts (especially on hydrology and agriculture), it is important that a weather generator or a statistical downscaling method reproduce different distributions such as the rainfall amount, the dry spell and the wet spell distributions. Figure 12 displays such comparisons using pp-plots and qq-plots. It is worth pointing out that, while the classification method is based on the entire dataset (i.e. the seasonal cycle is not explicitly separated before the classification), we made all plots by comparing observed and simulated monthly distributions at all stations allowing to evaluating the representation of the seasonal cycle by the method. Finally, considering that our simulations are ensembles of 100 simulations, we computed the simulated distributions as follows. First, for each month of each simulation of each station, we compute the dry sequence, wet sequence or rainfall amount CDF. Second, for each month and at each station, we average the CDFs between all the members of the ensemble before comparing to the observed monthly CDF.

First, the method is found to represent fairly well the dry spell distributions for all probabilities (Fig. 12a) although it clearly underestimates the dry spell lengths longer than 40 days by 30% to 50% (Fig. 12b). This bias is quite systematic in most of the weather generators (*Wilks, 1999; Boulanger et al., 2007*). A potential improvement of the method would be to take into account the weather pattern and precipitation history in the computation of the precipitation occurrence probability.

Second, coherently with the previous point, the statistical model significantly overestimates (Fig. 12c) the short rainfall spells, while it underestimates very long wet spells (longer than 10 days; Fig. 12d).

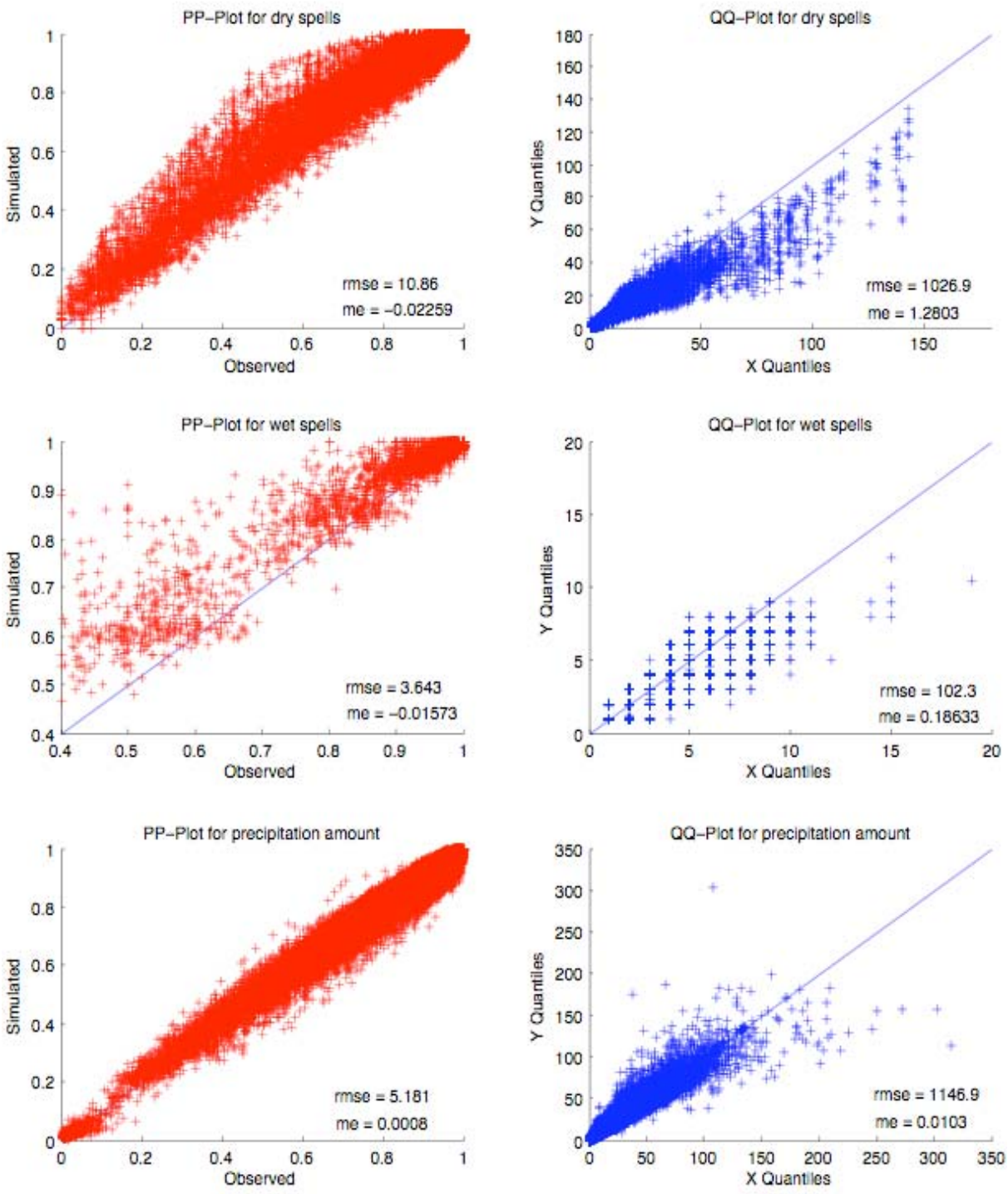

Figure 12: *(a: upper-left) PP-Plot of the dry sequences; (b: upper-right) QQ-Plot of the dry sequences; (c: middle-left) PP-plot of the wet sequences; (d: middle-right) QQ-plot of the wet sequences; (e: lower-left) PP-plot of the rainfall amounts; (f: lower-right) QQ-plot of the rainfall amounts. All plots are computed comparing the distributions of all twelve months at all stations.*

Third, rainfall amount distributions as displayed by Figures 12e-f seem to be fairly well simulated by the method confirming the skill of the method in simulating different amplitudes of rainfall events. Only in Figure 12f, it seems that the method does not reproduce very large specific daily rainfall events (larger than 200mm/day). This can actually be explained by the fact that all simulations over a specific year make use of a classification of weather patterns observed during all the period except this specific year. Therefore, very large individual events (not observed during the rest of the period) are unlikely to be simulated by the statistical method. When analyzing more closely the model sensitivity over different regions of Argentina, the RSS results at each station (Figure 13) confirm that the RSS values are very similar whatever the threshold suggesting that the statistical model skills are good either for low and large rainfall amounts. However, Figure 13 also displays regional differences. In particular, lower RSS values (0.55-0.6) are mainly observed near the Andes. We believe that such low scores can be explained by two reasons. First, these regions are quite dry, and thus small errors in precipitation occurrence or amounts (in terms of % of the distribution) can lead to lower scores. Second, the quality of the reanalysis can also be lower near the Andes, since its abrupt topography change is a clear challenge for atmospheric models. We believe that both reasons can lead to a transfer function not as skilful in relating weather patterns to local daily precipitation. In order to better describe such differences, in Figure 14 we display different daily precipitation time series with low RSS (Mendoza~0.6 and Rio Gallegos~0.5) or large RSS (Gualeguaychú on the Uruguay River ~0.75; and Marcos Juarez~0.70). At the first two stations, the 90-day filtered daily precipitation time series display very low precipitation amplitudes (lower than 4mm/day in Mendoza and 2mm/day in Rio Gallegos). In Mendoza, the seasonal cycle is quite strong and fairly well simulated by the model. However, the model fails in capturing some periods such as 1988, 1991, 1996 and 1998.

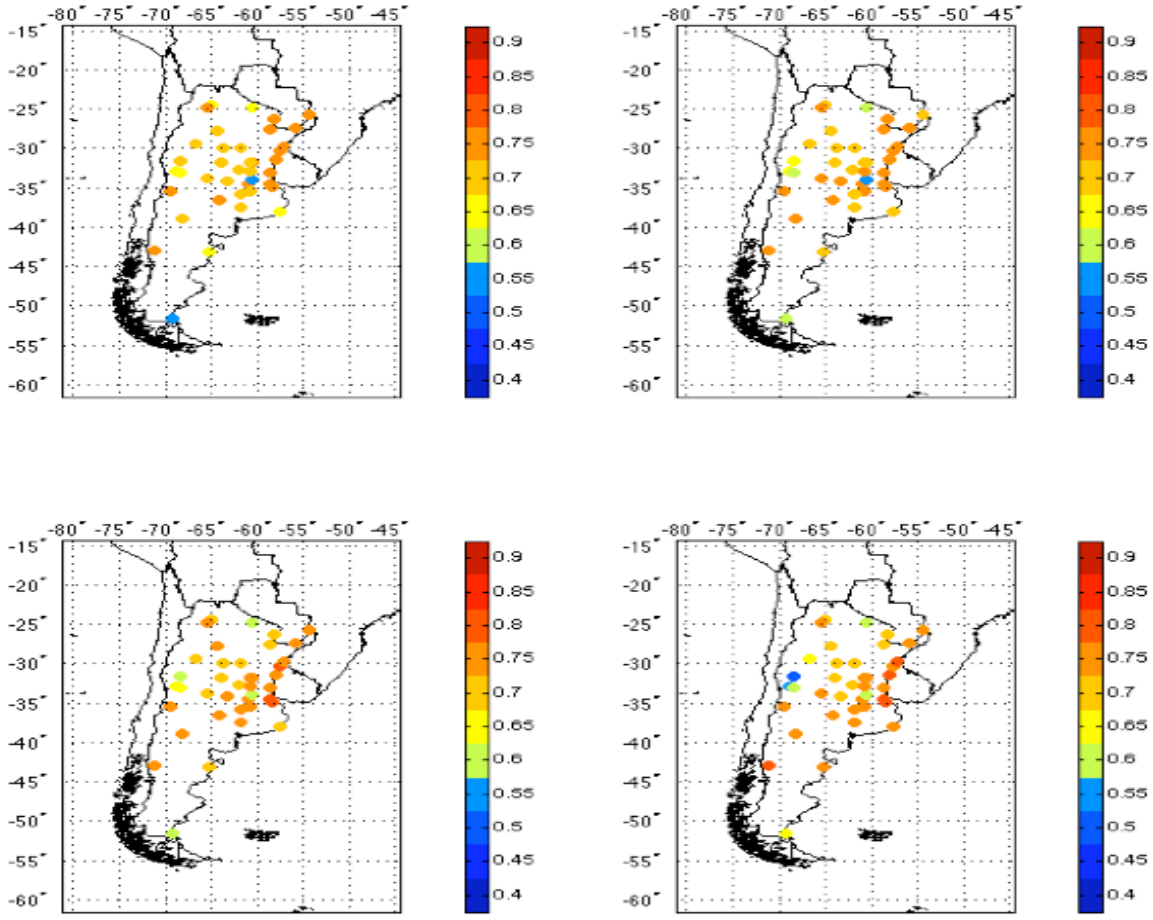

Figure 13: *ROC skill score (RSS) at each station. RSS is computed for four different criteria: (upper-left) wet/dry day; (upper-right) daily amount larger than the 25th percentile of the rainfall amount cumulative distribution function (CDF); (lower-left) daily amount larger than the 50th percentile; (lower-right) daily amount larger than the 75th percentile*

In Rio Gallegos, the seasonal cycle is not well defined, and the interannual variability is large, the statistical model clearly fails in representing the observed variability and, instead, displays a relatively smooth annual and interannual variability. On the contrary, at Gualeguaychú and Marcos Juarez stations with larger rainfall amplitudes the statistical method captures fairly well their strong annual and interannual variability. It is worth pointing out that even if the method fails in simulating some specific large peaks (related to individual large events), the green and pink curves (10th and 90th percentiles) follow pretty well the observed blue curve demonstrating that the ensemble does not present too large a spread in its simulations.

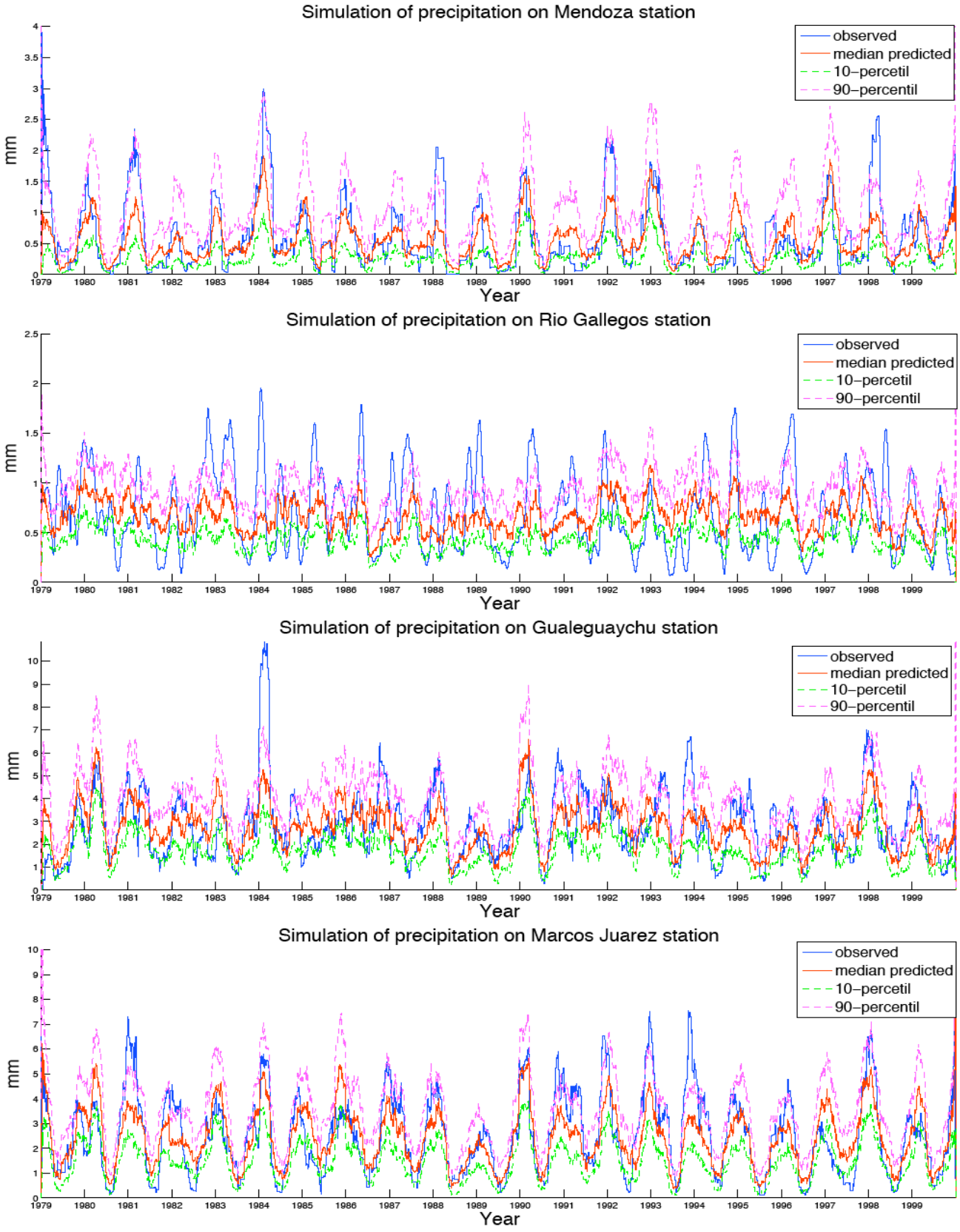

Figure 14: *Two-month filtered time series of observed daily precipitation (blue curve), of simulated ensemble median (red curve), of simulated ensemble 10th percentile (green curve) and of simulated ensemble 90th percentile (pink curve). From up to bottom, the time series correspond to Mendoza, Rio Gallegos, Gualeguaychú and Marcos Juarez.*

VI. Comparison with dynamical downscaling

VI. a. Dynamical models and period description

In order to compare the performance of our statistical model with the dynamical downscaling approach, we co-ordinated our efforts with the RCM groups within CLARIS. Three multi-model ensembles of simulations of particularly anomalous months in terms of precipitation in the southern La Plata Basin (January 1971, November 1986 and July 1996) were performed. The RCMs participating in this downscaling experiment are: MM5 (CIMA and UCH), RCA3 (CIMA and Rossby Centre/SMHI), REMO (MPI-M), PROMES (UCLM) and WRF (CIMA). LMDZ (LMD), an atmospheric GCM with variable grid spacing (stretched grid), run with high resolution over South America, also participates in these experiments. Concurrently, RCMs are being applied to study regional effects of global climate change in South America (*Núñez et al., 2006; Marengo, 2007; Fuenzalida, 2007; Sörensson et al., 2007*) and other regions. A short description of participating models is given in table 5. (Further information about the dynamical simulations models and the months of analysis presented here can be found in *Menéndez et. al. 2008*). The selection of the periods is based on *in situ* observational data studies for central and north-eastern Argentina (*Bettolli et al., 2005; Barrucand et al., 2001*). All dynamical regional simulations were initialized and forced every 6h by large-scale atmospheric boundary conditions from the European Centre for Medium-Range Weather Forecasts (ECMWF) 40-year Reanalysis (ERA40, *Uppala et al., 2005*). All models were run with horizontal resolution of about 50 km over South America but varying vertical resolution. The five regional models' domains are somewhat different from model to model but share southern South America and surrounding oceans.

Table 5: *Summary of grid configurations and parameterizations for the dynamical models used in the present study.*

	LMDZ	MM5	RCA3	REMO	PROMES	WRF
Reference	Hourdin et al. (2006)	Solman et al. (2007)	Kjellström et al. (2005)	Jacob (2001)	Castro et al. (1993)	http://www.mmm.ucar.edu/wrf/users/docs/arw_v2.pdf
Grid resolution	0.5° to 0.7°	50 km	50 km	0.5°	50 km	50 km
Grid (lat*lon)	100x97	110x130	155x134	121x145	139x145	101x150
Vertical levels	19	23	24	31	28	31
Convection	Emanuel (1993)	Kain and Fritsch (1993)	Kain and Fritsch (1993); Jones and Sanchez (2002)	Tiedtke (1989), modifications after Nordeng (1994)	Kain and Fritsch (1993)	Grell and Devenyi (2002)
Microphysics	Bony and Emanuel (2001)	Explicit moisture scheme (Hsie et al., 1984)	Rasch and Kristjansson (1998)	Sundquist (1978)	Hsie et al. (1984)	Eta Ferrier (New ETA microphysic) scheme
Radiation	Morcrette (1991)	Stephens (1978); Garand (1983)	Savijärvi (1990); Sass et al. (1994); Räisänen et al. (2000)	Morcrette et al. (1986); Giorgetta and Wild (1995)	Stephens (1978); Garand (1983)	Mlawer et al. (1997); Dudhia (1989)
Land surface	Krinner et al. (2005)	Noah Land Surface Model (Chen and Dudhia 2001)	Samuelsson et al. (2006); Champeaux et al. (2005)	Dümeniel and Todini (1992)	Ducoudre et al. (1993)	Noah land-surface model (Chen and Dudhia, 2001)
Soil thermal layers	11	3	5	5	7	4
Soil moisture layers	2	3	2	1	2	4

Simulations were evaluated against both station data and high-resolution (0.5º) precipitation data compiled, respectively, by the CLARIS Work Package 3.2 and the Climatic Research Unit (CRU) of the University of East Anglia (*New et al., 1999, 2000*). The station dataset consists of daily values of precipitation for 39 Argentine weather stations north of 39ºS.

The results are presented for southern South America (50ºS, 20ºS, 85ºW, 35ºW) and for three smaller regions of particular interest for this project in central and north-eastern

Argentina that we refer to as North-Eastern Argentina (NEA, 24ºS, 29ºS, 55.5ºW, 61ºW), Southern Mesopotamia (SME, 29ºS, 34ºS, 56ºW, 62ºW) and Central-Eastern Argentina (CEA, 34ºS, 38.5ºS, 56ºW, 62.5ºW). These regions and the observational stations that are used for comparison with model results are presented in Figure 15. Note that all considered stations are located over relatively flat and low terrain.

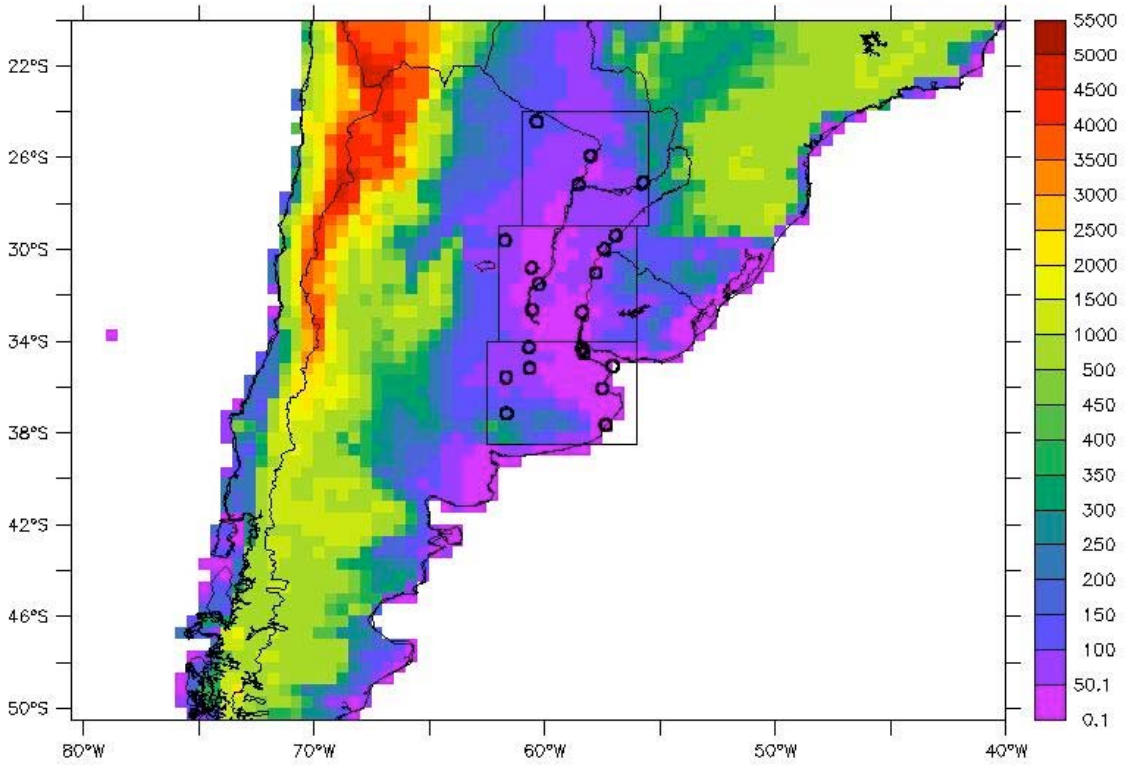

Figure 15: *Regional domain showing the topographic field, the three subregions used to compute statistical measures and the location of meteorological stations used for comparison with models results.*

VI.b. Frequency distribution of the daily rainfall rates

At this point an important question is the comparison of models' results with daily station data and with the statistical downscaling technique. The targets are twofold: to explore the extent to which using a statistical downscaling technique improves the downscaling of the distribution of precipitation in intensity classes, and to explore how both techniques (dynamical and statistical downscaling) capture the heaviest rainfall days. In order to answer the first issue, we made frequency diagrams of daily precipitation for each model, for the SDS and for the available observational data. For each individual model we count for each grid point in each sub-region (NEA, SME, CEA), the total number of days within each precipitation interval representing dry days or "drizzle" precipitation (0-1 mm/day) and light (1–5 mm/day), moderate (5–15 mm/day), strong (15–30 mm/day) and heavy (> 30 mm/day) precipitation days. Then we evaluate the mean frequency (in percentage) for the considered region during each analyzed period. The results are shown in figures 16-a, 16-b and 16-c, after averaging over models. The frequency distributions for the models are described by the median, the 25% and 75%, or quartile, values (half of the models lie between these two values) and the maximum and minimum values in the model ensemble. For the SDS and for the in situ data, the methodology is similar but we count for each station the number of days in each precipitation regime (we show the mean frequency for the considered region during each analyzed period).

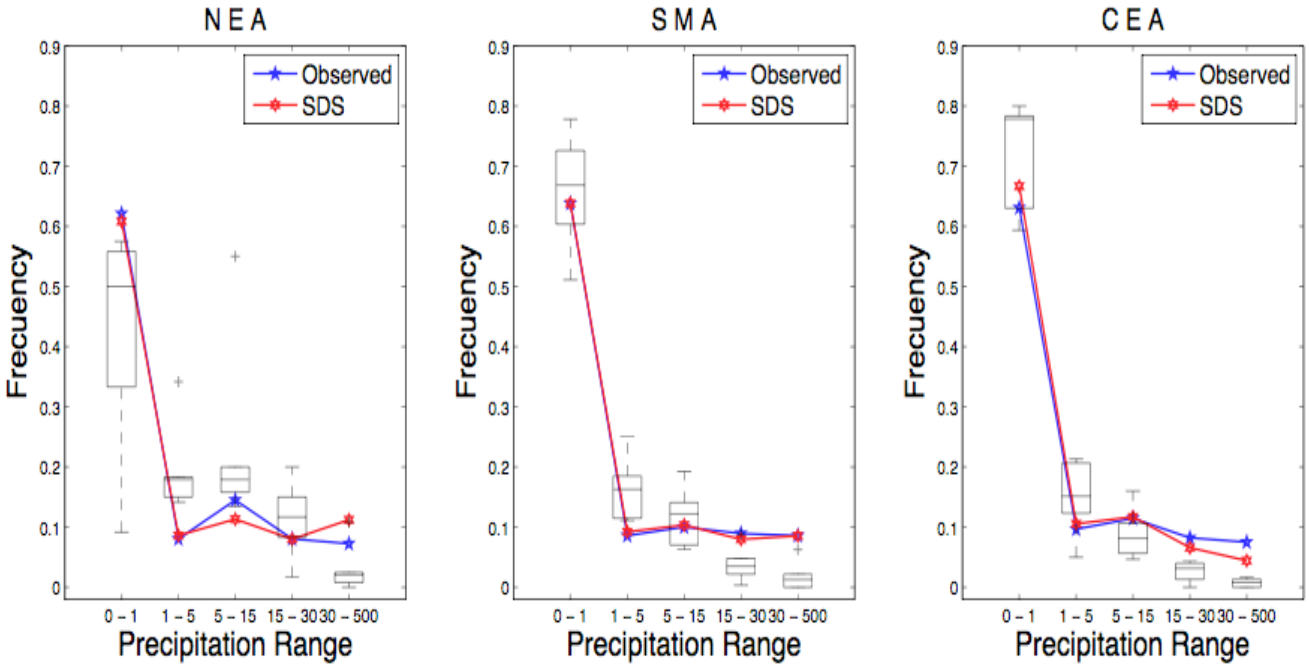

Figure 16-a: *Intermodel range of frequency of daily precipitation for the regions NEA, CME and CEA for January 1971. For each grid point and each model, we count the total number of days within each precipitation interval. For each interval, the figure shows the minimum, maximum, median and 25 and 75% quartile values among the six models. Blue lines represent observations from meteorological stations and the red lines represent the statistical downscaling results.*

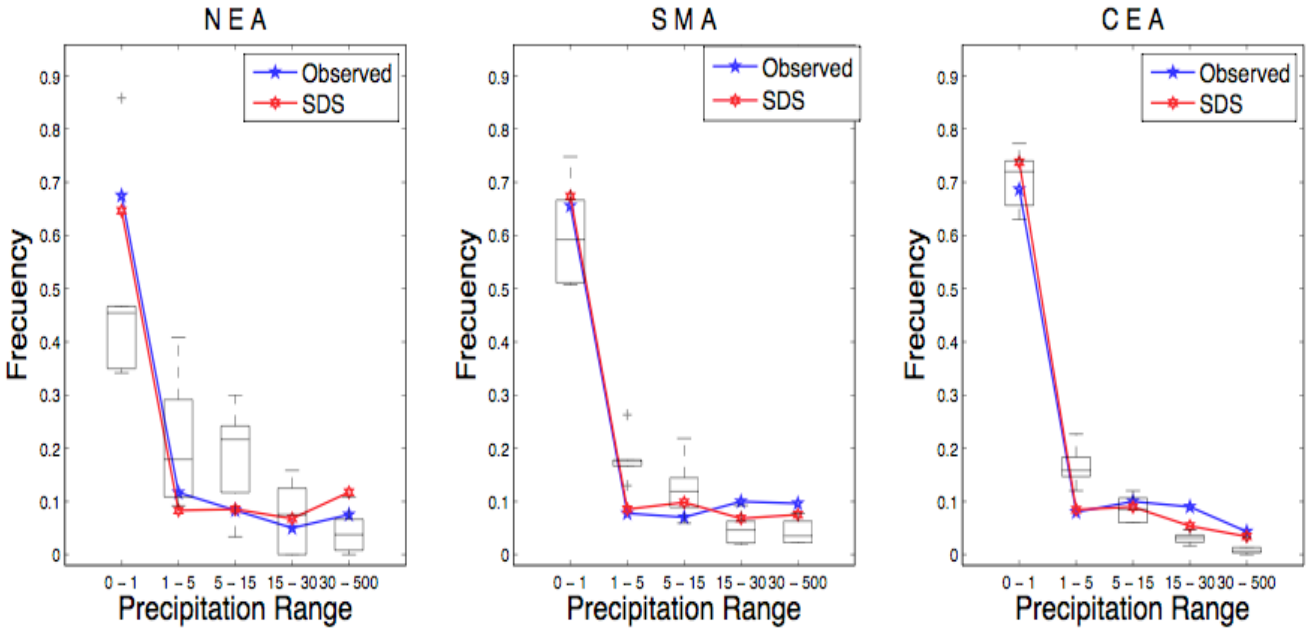

Figure 16-b: *As fig. 16-a, but for November 1986.*

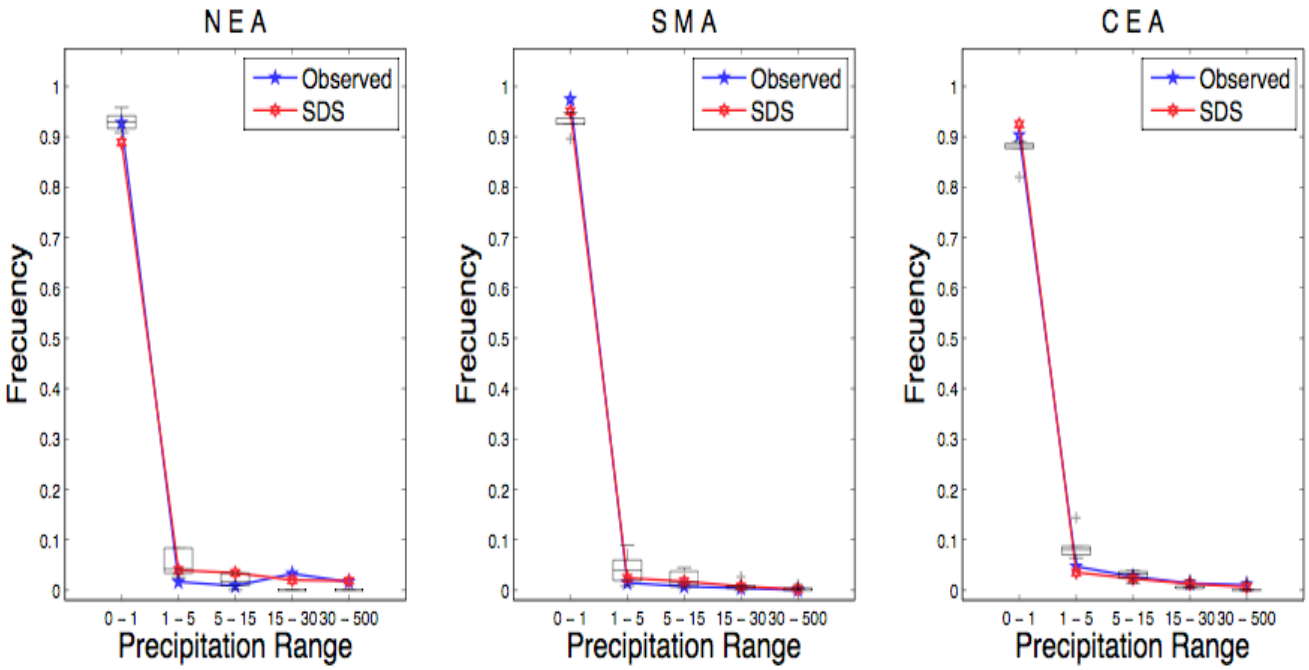

Figure 16-c: *As fig. 16-a, but for July 1996.*

In general, the frequency distribution of daily rainfall rates according to the SDS follows the overall features of those observed over the three regions and during the three periods (Figs. 16-a, 16-b and 16-c). The dynamical models' ensemble also seems to succeed in reproducing the overall observed frequency of daily precipitation for all regions and periods. At least, the observed frequency is often found within the min-max range of the ensemble and is at times found within the inter-quartile range. But we notice that most dynamical models tend to underestimate the frequency of dry days over NEA and overestimate the amount of light rainfall days in the three regions. As expected, the number of events in the higher intensity regimes tends to be under simulated by the models. During the first period (Fig. 16-a), the SDS always gives a better estimate of the frequency of rainfall in each range of amounts than the models or the mean of the models. However, the differences between observations and SDS estimates in the frequency of heavy precipitation days are quite noticeable. During the second period (Fig. 16-b), it is striking in NEA that the SDS simulates

much better the observation probability of dry days. During the third period (Fig. 16-c), which was not characterized by heavy rainfalls, the differences between the dynamical and statistical results are low. Overall, and especially during the first and second periods, the statistical model overcomes the dynamical ensemble in representing all ranges of precipitation amounts.

VI.c. Heavy rainfall comparison

In order to provide a better quantification, Tables 6a-c compare the simulated heavy rainfall, as defined by the 1-day monthly maximum precipitation, with corresponding values from the statistical downscaling technique and with station observations. For each sub-region (NEA, CME, CEA), we consider the 1-day monthly maximum precipitation at each station, and then we found the minimum and maximum of these quantities. Each min-max interval represents the range of rainfall amounts corresponding to the heaviest rainfall day in the stations of each sub-region for the observations, the models and the statistical downscaling.

Given that the SDS simulation is actually an ensemble of 100 simulations, the methodology to compare SDS and individual dynamical models require some adjustments. Thus, the SDS results are computed in two different ways. For both ways, first the maximum value of each simulation of the ensemble at each station is computed. Second, in the first case, we compute the maximum and minimum values of these maxima at each station, while, in the second case, we compute the 90% and 10% percentiles of these maxima at each station. Finally, the minimum and maximum values among all stations are computed and displayed in Tables 6a-c. The second case (selection of 90% and 10% percentiles) is considered as the stochastic nature of the SDS ensemble implying that for a large number of simulations, the SDS will simulate all values of the precipitation distribution, although with a probability influenced by the weather patterns observed during the simulated period. Thus, as noted in

Tables 6a-c, the range of values computed in the first case always include the observations although these extreme values may have a very low probability of occurrence. When computing the 90% and 10% percentiles, the range of values is much similar to the observations although the maximum values are systematically larger than observations. Despite of this, given the objective of comparison between individual dynamical models, SDS and observations, it can be concluded that the SDS reproduces fairly well the observations.

It is worth noting important remaining methodological issues related to comparing precipitation extremes from station observations with model grid-point values. In particular, care will have to be taken to assess the simulated precipitation extremes against station data because the level of variability in spatially averaged rainfall is not comparable to that of point rain-gauge observations. For example, a model that produces 24-hour precipitation events that are as large as found in station data would be somewhat suspect since local intensities measured by rain gauges should be greater than grid box mean intensities simulated by models (even in RCMs running at 50 km resolution).

Table 6a*: First period (January 1971). Range of 1-day monthly maximum precipitation for each sub-region (NEA, CME, CEA) as simulated by each model and from the statistical downscaling method (SDS) and station observations. SDS1 represents the results of the statistical model when computing first the maximum of each simulation of the ensemble at each station, second, the maximum and minimum of these maxima at each station and finally the minimum and maximum among all the stations. SDS2 represents the results of the statistical model when computing first the maximum of each simulation of the ensemble at each station, second, the 90% and 10% percentiles of these maxima at each station and finally the minimum and maximum among all the stations. Units: mm/d.*

JAN'71	**NEA**		**SME**		**CEA**	
	Min	**Max**	**Min**	**Max**	**Min**	**Max**
Observtions	43.6	67.4	59.9	151.6	11.3	128.1
LMDZ	11.3	27.1	9.0	66.5	11.1	53.4
MM5	14.8	55.2	3.9	28.2	4.2	32.6
REMO	27.7	36.6	5.9	51.8	10.1	48.6
RCA	21.1	44.5	16.4	46.8	12.0	29.3
PROMES	36.0	49.7	34.0	84.9	6.25	48.1
WRF	22.8	37.9	10.0	29.5	5.6	26.3
SDS1	16.0	209.0	16.0	302.7	0.3	138.0
SDS2	34.5	133.6	25.7	144.0	5.7	99.0

Table 6b: *Same as Table 6a but for the second period (November 1986).*

NOV'86	NEA		SME		CEA	
	Min	**Max**	**Min**	**Max**	**Min**	**Max**
Observtions	36.4	119.8	39.6	105.2	7.5	78.0
LMDZ	6.3	78.6	19.1	72.3	8.6	50.0
MM5	63.8	127.7	9.7	82.8	3.9	32.0
REMO	33.5	94.2	49.4	199.0	4.9	87.7
RCA	17.1	37.2	16.9	66.6	6.9	42.2
PROMES	34.9	53.9	10.1	52.1	9.8	30.7
WRF	1.1	7.2	22.5	75.8	5.2	26.1
SDS1	18.8	209.0	12.5	315.0	4.0	225.3
SDS2	36.0	183.8	22.0	165.8	8.0	92.0

Table 6c: *Same as Table 6a, but for the third period (July 1996).*

JUL'96	NEA		SME		CEA	
	Min	**Max**	**Min**	**Max**	**Min**	**Max**
Observations	2.0	34.0	0.0	20.0	3.0	39.0
LMDZ	1.4	6.4	2.0	23.8	3.7	25.7
MM5	4.4	9.8	6.7	20.6	6.3	25.7
REMO	1.3	4.2	3.7	67.5	2.7	61.6
RCA	1.0	5.0	1.7	9.9	2.6	18.7
PROMES	3.7	9.7	9.0	31.3	8.1	29.6
WRF	1.3	6.0	8.3	28.1	3.9	19.1
SDS1	0	89.5	0.0	66.4	0	95.1
SDS2	0.5	73.0	0.0	31.0	0.0	74.0

VII. Conclusion and perspectives

Very few studies (e.g. *Solman and Nuñez, 1999; Gutierrez et al., 2004*) have developed and used statistical downscaling methods to predict daily precipitation at local scale (weather station) in South America. The present study is a contribution to fill this gap. We developed and calibrated a weather pattern clustering technique using the 1979-1999 ERA-40 atmospheric reanalysis and a set of 39 quality-controlled weather stations in Argentina. The variety of climates observed in Argentina gives us the opportunity to develop a method valid either for the north of the country (tropical climate), for the south (mid- to high-latitude climate), for the west (near the Andes), for the east (Atlantic Ocean coast) and for the interior of the country.

First, the method parameters were optimized based on the RSS:

(i) ***The clustering technique***: A comparison between the k-means and the SOM (Self-Organizing Map) clustering methods led to the conclusion that the SOM topological order reduced the possibility for the clusters to represent well all the data space (especially regions of low density) and therefore the generalization skill of the projection method.

(ii) ***The number of clusters or average number of observations per cluster***: The RSS was found to be optimum for an average number of observations per cluster larger than 39. For lower values, the generalization skill of the clustering analysis reduces significantly the RSS. For very large values, the same applies as too many weather states are mixed in a same cluster leading to a loss in predictive information. We decided to use 196 clusters equivalent to an average of 39 observations per cluster.

(iii) ***The domain size***: First (not shown), no significant sensitivity to the location was found in the computation of an optimum domain size to extract the atmospheric variables and thus to define the weather pattern. It was found that the optimum domain size was relatively small (~4° to 6° square around the station). Moreover, the same analysis reducing the atmospheric variables to dynamical only variables led to the conclusion that the optimum domain size depends on the atmospheric variables. Indeed, dynamical variables define an optimum transfer function if the domain size is larger (~10°) suggesting that our results with all variables together is strongly influenced by local- to synoptic-scale non-dynamical variables (moisture component). It also suggests that dynamical and non-dynamical variables should be defined onto different domains.

(iv) ***Ensemble size*****:** As any stochastic method, it is necessary to compute an ensemble of simulations. The RSS is found to converge rapidly to a maximum value when the number of simulations is larger than twice or thrice the average number of

observations per cluster. This result is coherent with the fact that, in such a case, for each day, the ensemble of simulated values does explore all the distribution of daily values in each cluster.

With such an optimization of the statistical method, the skill was found to be relatively homogeneous all over the country despite some lower results near the Andes, probably due to a topography effect, which may affect the transfer function between ERA-40 reanalysis near-Andes weather patterns and daily precipitation. The RSS for different criteria (wet/dry days, days with rainfall larger than the 25^{th}, 50^{th} or 75^{th} percentiles of the rainfall amount CDF) is found to be relatively stable (around 0.72 for the entire database and for each criterion). More interestingly, while the method does not explicitly separate the seasonal cycle characteristics, the simulated monthly CDFs of wet spells, dry spells and rainfall amounts do compare fairly well to the observed CDFs. The major weakness of the method is its underestimation of either long dry or wet spells. Such a weakness is similar to other methods or to weather generators. Finally, the analysis of the observed and simulated time series allows concluding that the method has less skill in arid regions than in semi-arid or wet regions. Indeed, in arid regions, small errors in the simulation of the amplitude of rainfall events (defined as percentiles of the distribution) do strongly affect the statistical scores. In the opposite, in wetter regions, the regimes of precipitation (weak vs. large amplitude) and their variability (seasonal, interannual) are much better captured and simulated by the statistical method, furthermore, despite this actual performance we can see that the statistical model outperforms the dynamical model in representing all ranges of precipitation amounts, especially during the first and second periods showed is this study.

The simulation of particular month-long cases characterized by extreme precipitation conditions in the southern La Plata Basin (January 1971, November 1986 and July 1996) showed that the statistical model outperforms the dynamical model in representing all ranges

of precipitation amounts, especially during the first and second periods, moreover, it outperforms rainfall frequency for all periods and range of precipitation.

To conclude, the present method could be improved in the following ways. First, as we found that dynamical and non-dynamical variables relate to the local precipitation through weather patterns of different spatial sizes, an improvement would thus be to combine different spatial domains associated to the different types of variables (dynamical and non-dynamical). Second, in this first version, during a simulation, a daily weather pattern is projected onto the clusters and only one "winning" cluster is considered (the one with the lowest distance). Then to simulate the precipitation, all observations belonging to the winning cluster are equally probable. The introduction of the weather pattern and/or precipitation history in conditioning the probability of each precipitation observation may improve our simulations, at least the simulations of long dry and wet spells. Last, it could be possible to relax the "winning" cluster condition by defining a probability function based on the distance to all the clusters. This "relaxation" complementary to the second possible improvement, may allow to better represent the probability of specific rainfall events and, in particular, extreme events. Such improvements will be tested in the framework of the CLARIS LPB Project (2008-2012) funded by the 7th Framework programme of the European Commission.

Appendix A: Atmospheric variables description

Millibars(mb)

Is a common measure of the air pressure, which is the weight of the column of air above a designated area. The average sea level pressure is 1010 mb.

U, V, W wind speed component

Wind speed is a term applied when talking about the movement of air from one place to the next. Technically, wind speed *ws* is given by,

$$|ws| = \sqrt[2]{U^2 + V^2 + W^2}$$

Where U, V, and W are zonal, meridional, and vertical components of wind velocity.
The terms zonal and meridional are used to describe directions on the globe. Zonal means "along a latitude circle" or "in the east-west direction"; while meridional means "along a meridian" or "in the north-south direction". For vector fields (such as wind speed), the zonal component (or x-coordinate) is denoted as U, while the meridional component (or y-coordinate) is denoted as V.

Mean sea level pressure (msl)

Mean sea level pressure is the pressure at sea level or (when measured at a given elevation on land) the station pressure reduced to sea level assuming an isothermal layer at the station temperature. The reduction to sea level means that the normal range of fluctuations in pressure is the same for everyone. The pressures which are considered high pressure or low pressure do not depend on geographical location. This makes isobars on weather map meaningful and useful tools.

Relative Humidity

Relative humidity (r) is the ratio of the amount of water vapor actually in the air compared to the maximum amount of water vapor the air can hold at that particular temperature and pressure

Specific Humidity

It is the ratio of the weight of water vapor in a specified volume to weight of the air in that same volume.

Total Colum Water (tcw)

It is a measure of the total amount of water in a column of air from ground pressure level to zero pressure level.

Geopotential height

Is a vertical coordinate referenced to Earth's mean sea level — an adjustment to geometric height (elevation above mean sea level) using the variation of gravity with latitude and elevation. Thus it can be considered a "gravity-adjusted height." One usually speaks of the geopotential height of a certain pressure level, which would correspond to the geopotential height necessary to reach the given pressure. At an elevation of h, the geopotential is defined as, $\Phi = \int_0^h g(\varphi, z)dz$ where g(φ,z) is the acceleration due to gravity, φ is latitude, and z is the geometric elevation. Thus, it is the gravitational potential energy per unit mass at that level. The geopotential height is, $Z_g = \frac{\Phi}{g_0}$, where g_0 is the standard gravity at mean sea level.

.

References

Bony S., Emanuel KA A., parameterization of the cloudiness associated with cumulus convection; evaluation using TOGA-COARE data. J Atmos Sci 58(21):3158–3183,2001.

Boulanger, J.-P., Fernando Martinez, Olga Penalba and Enrique Carlos Segura, Neural network based daily precipitation generator (NNGEN-P), Clim. Dyn., DOI 10.1007/s00382-006-0184-y, 2007.

Cavazos, T., Using Self-Organizing Maps to Investigate Extreme Climate Events: An Application to Wintertime Precipitation in the Balkans, J. Clim. 13, 1718-1732, 2000.

Cavazos T, and B. C. Hewitson, Performance of NCEP-NCAR reanalysis variables in statistical downscaling of daily precipitation. Climate Research Vol. 28:95-107, 2005.

Champeaux J.L., Masson V., Chauvin F. ECOCLIMAP: a global database of land surface parameters at 1 km resolution. Meteorol Appl 12: 29-32,2005.

Chen F., Dudhia J., Coupling and advanced land surface-hydrology model with the Penn State-NCAR MM5 modeling system. Part I: Model implementation and sensitivity. Mon Wea Rev 129: 569-585,2001.

Ducoudre N., Laval K., Perrier A. SECHIBA, a new set of parameterizations of the hydrologic exchanges at the land-atmosphere interface within the LMD atmospheric general circulation model. J Clim 6:248-273,1993.

Dudhia J., Numerical study of convection observed during the winter monsoon experiment using a mesoscale two-dimensional model. J Atmos Sci 46:3077-3107,1989.

Dümenil L., Todini E. , A rainfall–runoff scheme for use in the Hamburg climate model. In: O'Kane JP (ed) Advances in theoretical hydrology, EGS series of hydrological sciences 1, Elsevier pp 129–157,1992.

Emanuel KA., A scheme for representing cumulus convection in large-scale models. J Atmos Sci 48:2313-2335,1993.

Fuenzalida H., Climate change simulations with PRECIS over Chile. Presentation at the CLARIS Final Meeting, La Plata, Argentina, June 2007

Garand L., Some improvements and complements to the infrared emissivity algorithm including a parameterization of the absorption in the continuum region. J Atmos Sci 40:230-244,1983.

Giorgetta M., Wild M., The water vapour continuum and its representation in ECHAM4, Max Planck Institut fuer Meteorologie Report vol 162, p38,1995.

Grell G.A., Dévényi D., A generalized approach to parameterizing convection combining ensemble and data assimilation techniques. Geophys Res Lett 29, 1693, doi:10.1029/2002GL01531,2002

Gutiérrez J. M, Cano R., Cofiño A. S. and C. Sordo, Analysis and Downscaling Multi-Model Seasonal Forecast using Self-Organizing Maps, Tellus, 2004.

Hewitson B.C., Crane R.G, Consensus between GCM climate change projections with empirical downscaling: Precipitation downscaling over South Africa, Int. J. Climatology, 2006.

Hourdin F., Musat I., Bony S., Braconnot P., Codron F., Dufresne J-L., Fairhead L., Filiberti M-A., P Friedlingstein, J-Y. Grandpeix, G. Krinner, P. LeVan, Z-X Li, F. Lott., The LMDZ4 general circulation model: climate performance and sensitivity to parametrized physics with emphasis on tropical convection. Clim Dyn 27:787-813,2006.

Hughes, J., Lettemaier, D. P., and Guttorp, P. A stochastic approach for assessing the effect of changes in regional circulation patterns on local precipitation. Water Resources Research, 29:3303–3315, 1993.

Jacob D., A note on the simulation of the annual and inter-annual variability of the water budget over the Baltic Sea drainage basin. Met Atmos Phys 77:61-73,2006.

Kain J., Fritsch J., Convective parameterization for mesoscale models: The Kain-Fritsch scheme. In Emanuell KA, Raymond DJ (eds) The representation of cumulus convection in numerical models. Amer Meteor Soc, Boston, pp 165-170,1993.

Kharin, V. V., and F. W. Zwiers, On the ROC score of probability forecasts, J. Clim., 2003.

Kjellström E., Bärring L., Gollvik S., Hansson U., Jones C., Samuelsson P., Rummukainen M., Ullerstig A., Willén U., Wyser K. , A 140-year simulation of European climate with the new version of the Rossby Centre regional atmospheric climate model (RCA3). Reports Meteorology and Climatology No. 108, SMHI, SE-60176 Norrköping, Sweden, 54pp,2005.

Kohonen, T, Self-Organizing formation of topologically correct feature maps. Biological Cybernetics, 43(1):59-69, 1982.

Krinner G., Viovy N., de-Noblet-Ducoudré N., Ogée J., Polcher J., Friedlingstein P., Ciais P., Sitch S., Prentice C., A dynamic global vegetation model for studies of the coupled atmosphere-biosphere system. Global Change Biology 19:1015:1048,2005.

Lorenz, E. N. Atmospheric predictability as revealed by naturally occurring analogues. Journal of Atmospheric Sciences, 26:636-646, 1969.

Marengo J.A., Integrating across spatial and temporal scales in climate projections: Challenges for using RCM projections to develop plausible scenarios for future extreme events in South America for vulnerability and impact studies. In: Meeting Report (Papers) of the IPCC TGICA Regional Expert Meeting, Nadi, Fiji, 20-22 June 2007

Mehrotra, R., and A. Sharma, A nonparametric nonhomogeneous hidden Markov model for downscaling of multisite daily rainfall occurrences, J. Geophys. Res., 110, D16108, doi: 10.1029/2004JD005677, 2005.

Menéndez C.G., De Castro M., Boulanger J.-P. , D'Onofrio A. E., Sanchez E., Sörensson A. A., Blazquez J. , Elizalde A., Jacob D., Le Treut H., Li Z. X., Núñez M. N., Pfeiffer S., Pessacg N., Rolla A:, M. Rojas, P. Samuelsson , S.A. Solman , C. Teichmann : Submited to Climate Change (CLARIS special issue)

Menéndez CG, Cabré MF, Nuñez MN (2004) Interannual and diurnal variability of January precipitation over subtropical South America simulated by a regional climate model. CLIVAR Exchanges 29

Mlawer E.J., Taubman S.J., Brown P.D., Iacono M.J., Clough S.J., Radiative transfer for inhomogeneous atmospheres: RRTM, a validated correlated-k model for the longwave. J Geophys Res 102D:16663–16682,1997.

Morcrette J.-J., Radiation and cloud radiative properties in the ECMWF operational weather forecast model. J Geophys Res 96D:9121-9132,1991.

Núñez M, S Solman, M Cabré (2006) Mean climate and annual cycle in a regional climate change experiment over Southern South America. II: Climate change scenarios (2081-2090). In: Proceedings of 8 ICSHMO, Foz do Iguacu, Brazil, April 24-28, 2006, 325-331

Räisänen P., Rummukainen M., Räisänen J., Modification of the HIRLAM radiation scheme for use in the Rossby Centre regional atmospheric climate model. Report No. 49, Department of Meteorology, University of Helsinki, 71 pp ,2000.

Samuelsson P., Gollvik S., Ullerstig A., The land-surface scheme of the Rossby Centre regional atmospheric climate model (RCA3). Report in Meteorology 122, SMHI. SE-601 76 Norrköping, Sweden,2006.

Sass B.H., Rontu L., Savijärvi H., Räisänen P., HIRLAM-2 Radiation scheme: Documentation and tests. Hirlam technical report No 16., SMHI. SE-601 76 Norrköping, Sweden, 43 pp,1994.

Savijärvi H., A fast radiation scheme for mesoscale model and short-range forecast models. J Appl Met 29:437-447,1990.

Solman S., Nuñez M,. Cabré M.F., Regional Climate change experiments over southern South America. I: Present climate. Clim Dyn DOI 10.1007/s00382-007-0304-3,2007.

Solman S. A., Nuñez Mario N., Local estimates of global climate change: A statistical downscaling approach. Int. J. Climatology 19:835-861, 1999.

Sörensson AA, CG Menéndez, U Hansson, P Samuelsson, U Willén (2007) Present and future climate as simulated by Rossby Centre Regional Atmosphere Model (RCA3) forced by ECHAM5-OM over South America. Presentation at the CLARIS Final Meeting, La Plata, Argentina, June 2007

Stephens G.L. , Radiation profiles in extended water clouds: II. Parameterization schemes. J Atmos Sci 35: 2123-2132,1978.

Tiedtke M. A comprehensive mass flux scheme for cumulus parameterization in large scale models. Mon Wea Rev 117:1779-1800,1989.

Vrac, M., M. L. Stein, K. Hayhoe, and X.-Z. Liang, A general method for validating statistical downscaling methods under future climate change, Geophysicial Research Letters, Vol. 34, L18701, doi:10.1029/2007GL030295, 2007

Wilby, R. L., T. M. L. Wigley, D. Conway, P. D. Jones, B. C. Hewitson, J. Main, and D. S. Wilks , Statistical Downscaling of General Circulation Model Output: A Comparison of Methods, WATER RESOURCES RESEARCH, Vol. 34, No. 11, 2995–3008, 1998.

Wilks, D. S., Interannual variability and extreme-value characteristics of several stochastic daily precipitation models, Agric and Forest Meteor., 93, 153-169, 1999.